Dynamic Adsorption Studies of Organic Iodine Species on Mordenites

A Thesis
Presented in Partial Fulfillment of the Requirements for the
Degree of Master of Science
with a
Major in Chemical Engineering
in the
College of Graduate Studies
University of Idaho
by
Tejaswini Ravindra Vaidya

Major Professor: Vivek Utgikar, Ph.D., P.E
Committee Members: Haiyan Zhao, Ph.D., P.E.; Krishnan Raja, Ph.D., P.E.
Department Administrator: Ching-An Peng, Ph.D.

December 2020

Authorization to Submit Thesis

This thesis of Tejaswini Ravindra Vaidya submitted for the degree of Master of Science with a Major in Chemical Engineering and titled "Dynamic Adsorption Studies of Organic Iodine Species on Mordenites," has been reviewed in final form. Permission, as indicated by the signatures and dates below, is now granted to submit final copies to the College of Graduate Studies for approval.

Major Professor: _____ Date: _____
Vivek Utgikar, Ph.D., P.E

Committee Members: _____ Date: _____
Haiyan Zhao, Ph.D., P.E

_____ Date: _____
Krishnan Raja, Ph.D., P.E.

Department
Administrator: _____ Date: _____
Ching-An Peng, Ph.D.

Abstract

Off – gas stream from used nuclear fuel recycling operations comprises of various contaminants such as ^{3}H, ^{14}C, ^{85}Kr, ^{131}I, and ^{129}I. Radioactive iodine, ^{129}I, is of significant concern due to its tendency to form hard-to-capture toxic volatile organic compounds such as methyl iodide, half-life in excess of 15 million years, and tendency to accumulate in human thyroid glands. It also has adverse impacts on the environment due to its toxic nature. Organic iodides can be hazardous even at ppb level concentrations, and hence the capture of ^{129}I is extremely important. Various methods such as absorption and adsorption have been employed in the past to capture volatile iodine species. Recent studies have been focusing on the adsorption of iodine species using solid porous adsorbents, and the current work involves the capture of organic iodine species on mordenites.

The off-gas environment was simulated using ppb level concentration of iodine species and the dynamic adsorption experiments were conducted to determine the efficiency of mordenites as adsorbents. Three different mordenites - sodium mordenite, partially exchanged silver mordenite, and fully exchanged silver mordenite were used as adsorbents. The silver mordenites were synthesized by ion exchange between silver nitrate solution and sodium mordenite and subjected to structural and compositional analysis. Adsorption-desorption cycles at different temperatures and using different materials of construction for the column were conducted and the effect of silver content on the adsorption capacity of sorbents was determined.

The sorption columns exhibited behavior atypical of pure adsorption with no breakthrough and exhaustion of the adsorbents. It was hypothesized columns were behaving as reactors operating at a steady-state. Kinetic analysis of the system was conducted incorporating the effects of diffusion and mass transfer. The analysis indicates that a second-order reaction was the rate-controlling mechanism for methyl iodide removal.

These research findings could give good insights about the behavior of volatile organic iodine species at lower concentrations and their effective capture.

Acknowledgments

It gives me immense pleasure in acknowledging the help extended by teachers, supporting staff, colleagues. This report would be incomplete if I don't convey my sincere thanks to all those who were involved.

First and foremost, my gratitude to my advisor Prof. Dr. Vivek P. Utgikar for his kind support in developing this project, without him I could not be able to complete this project.

I am grateful to my committee members Dr. Haiyan Zhao and Dr. Krishnan Raja for their valuable feedbacks.

I am very much thankful to Dr. John P. Stanford who executed his post-doctoral work to help this research and for supporting me at the conception of this project and strengthening my resolve in so many direct and indirect ways.

I would also like to thank Dr. Dave Macpherson, Nicolene Van Rooyen, Lucas Arnold, Kelty Shroyer, Chaithanya Balumuru, Charles Cornwall, Aaron Babino for their technical help, Gail Bergman and Margaret Baker for their assistance, and my mates who have helped me in any manner, direct or indirect, in the completion of this monograph.

Table of Contents

List of Tables

List of Figures

Chapter 1: Introduction and Literature Review

In this chapter, a scenario about today's nuclear energy, an outline of commercial nuclear power plants, and the previous studies related to radioactive waste management are discussed.

1.1 Nuclear Energy today

There are 442 operable nuclear reactors in the world which produced 2657 TWh electricity in 2019 which was the second-highest output by nuclear energy after 2006 [1]. The United States has been using nuclear energy for over 60 years for energy generation and national defense purposes [2] [3]. About 19.7% of the United States electricity is produced by nuclear energy as shown in figure 1 [4]. The United States has 94 operable nuclear reactors with a combined capacity of 0.0972 TWe and 2 reactors are under construction having the combined capacity of 0.002234 TWe [1]. All commercial nuclear reactors in the United States are PWRs (pressurized water reactors) and BWRs (boiling water reactors) which fall under the category of light water reactors [5]. Among these, there are 63 pressurized water reactors (PWR) and 31 boiling water reactors (BWR) [5].

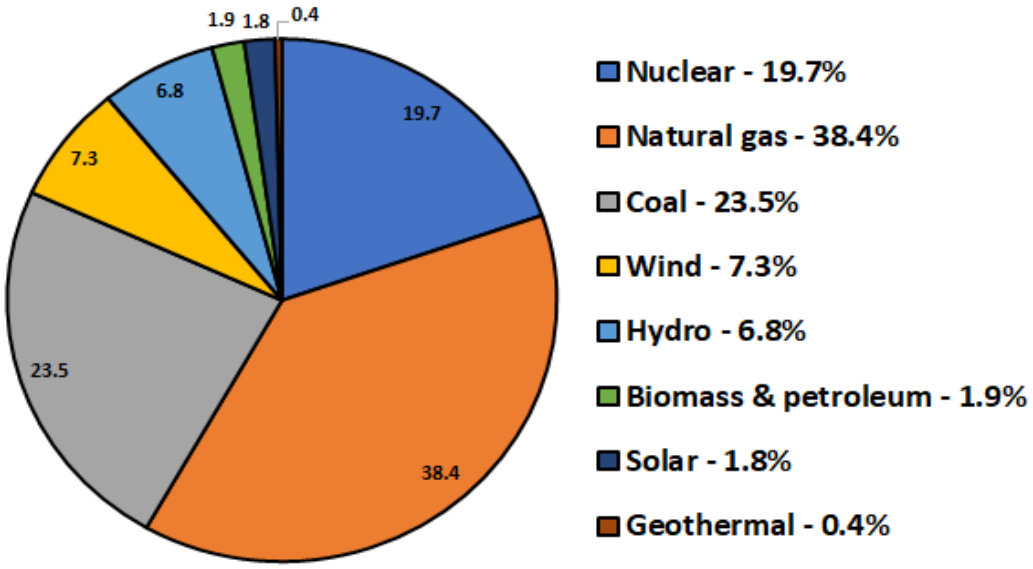

Figure 1: The United States electricity production as of 2019 [4]

Nuclear energy can be considered clean and sustainable because unlike other forms of energy, it does not have harmful impacts on the environment associated with the emission of greenhouse gases [6]. Evidently, in the United States, nuclear energy usage circumvents the emissions of 506 million metric tons of CO_2, 238,084 short tons of NO_X, and 265,260 short tons of SO_2 [4]. 809.4 TWh of electricity has been produced by nuclear energy in the United States in the year 2019 [4]. One of the advantages of nuclear energy over other forms of energy is the efficient capacity factor. The capacity factor is crucial for interpreting the efficiency of any energy plant. The capacity factor is the ratio of actual generated energy and the maximum capability of the energy generation of the plant [7]. As of

2019, nuclear plants had a 93.4% capacity factor, which is better than coal, natural gas, wind energy, and solar energy plants [4]. Due to these benefits of nuclear energy over other forms of energy, nuclear energy evolution can be expected in the upcoming years [8].

1.2 An overview of a typical nuclear power plant

A nuclear power plant is a thermal power plant in which the heat source is nuclear energy [9]. The energy generation through nuclear power plant is a two-step process involving steam generation by nuclear energy and electricity production by steam-driven generators [9]. A typical nuclear power plant is comprised of various components classified as nuclear and non-nuclear [9]. Non-nuclear components include heat exchangers, turbines, cooling towers, condensers, and electricity generators [9]. The nuclear component includes a nuclear reactor which includes components such as nuclear fuel, control rods, reactor core, containment, and coolant [9].

1.2.1 Nuclear fission chain reaction

The production of electricity through nuclear power involves a nuclear fission reaction as shown in figure 2 [9]. The nuclear fission reaction takes place inside the core of a nuclear reactor [9]. The liberated heat from the nuclear reaction helps to convert water into steam [9].

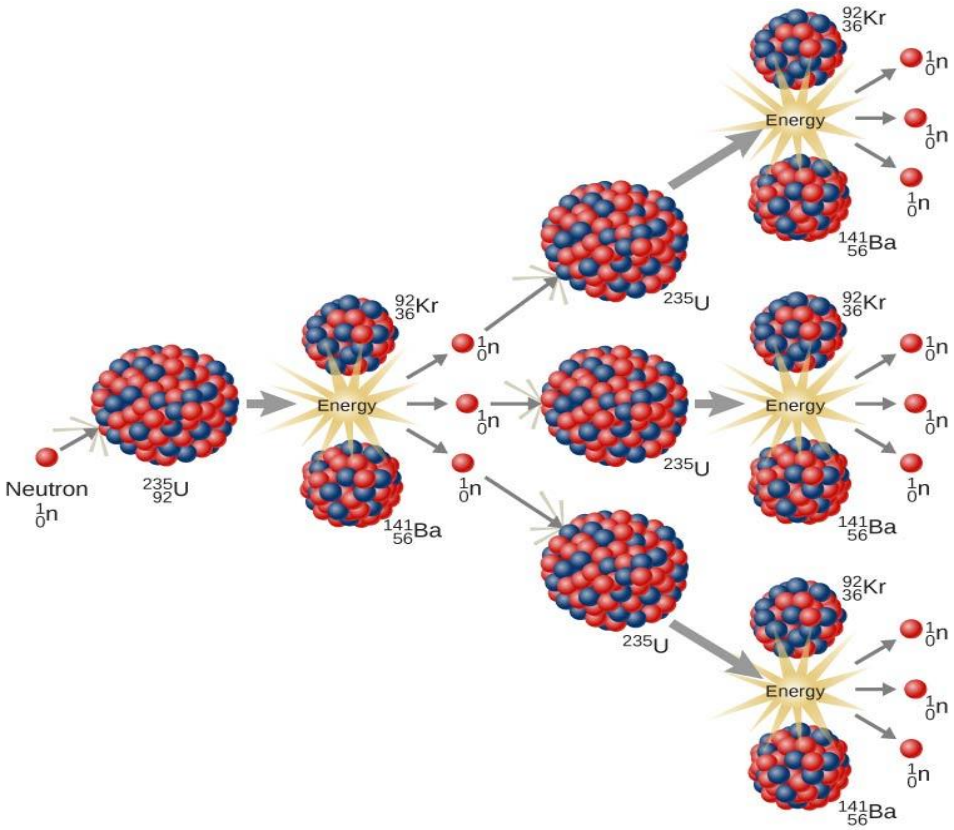

Figure 2: Nuclear fission reaction [10]

In a nuclear fission reaction, a heavy atom such as ^{235}U is bombarded by a neutron and the nucleus gets split into two lighter atoms with the release of more neutrons [9]. These neutrons collide with other uranium nuclei that split and the process continues with the release of a tremendous amount of energy [9]. The fission reaction is characterized by 'multiplication factor, k' which is the ratio of the number of fission neutrons liberated in one generation and the number of fission neutrons generated in previous generations [9]. The fission reaction is controlled by this multiplication factor [9]. If 'k' is greater than 1, the chain reaction is supercritical because the energy liberation increases with time [9]. If 'k' is less than 1, the reaction is subcritical because the energy liberation decreases with time [9]. If 'k' equals 1, the reaction is stable and critical [9]. According to the desired power generation demand, a multiplication factor is manipulated [9].

1.2.2 Nuclear reactors in the United States

A nuclear reactor is the most important component in the first step of power generation [9]. Nuclear reactors can be classified as light water reactors, heavy water reactors, gas-cooled reactors, molten salt reactors [9]. Light water reactors can be further classified as a pressurized water reactor (PWR) and boiling water reactor (BWR) [9]. PWR and BWR operate on different principles as described below.

1.2.2.1 Pressurized water reactor (PWR)

A pressurized water reactor is the most common nuclear reactor in the United States [5]. A PWR assembly consists of a reactor vessel, steam generators, pressurizer, and coolant pumps [9]. As shown in figure 3(a), water enters at 290°C into the reaction vessel and passes through the core where it gets heated due to liberated heat from fission reaction and leaves the vessel around 325°C [9]. This water is kept under pressure of 15 MPa in a reactor to avoid boiling of water [9].

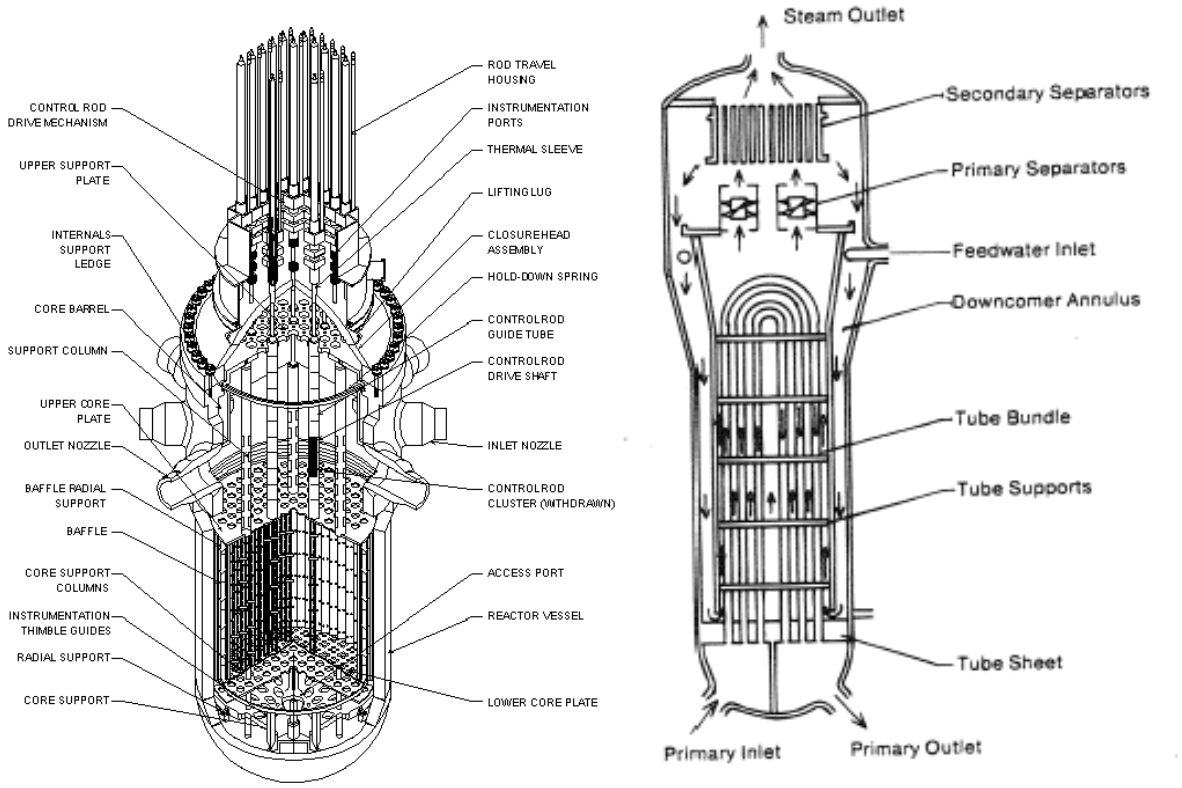

(a) (b)

Figure 3: (a) a schematic of PWR [9] (b) Steam generator [9]

The water then enters the steam generator which is a U-tube shell and tube heat exchanger to produce steam as shown in figure 3(b) [9]. The pressurized heated water from the reactor goes through thousands of U-tubes [9]. The shell side of the heat exchanger is filled with cool water returning from the turbine condenser [9]. The heat is transferred from the tube side water to shell side water and thereby producing steam [9]. Before leaving the generator, the steam passes through moisture separators and the condensate returns to the shell side [9]. If the volume of water in the reactor changes it would adversely affect the system leading to the burning of fuel elements [9]. To maintain the pressure, a surge tank called a pressurizer is placed [9]. This pressurizer is filled with steam at the upper section and water at the bottom section as shown in figure 4(a) [9]. This tank has pressure operated water spray nozzle at the upper section and pressure-actuated immersion heaters at the bottom section [9].

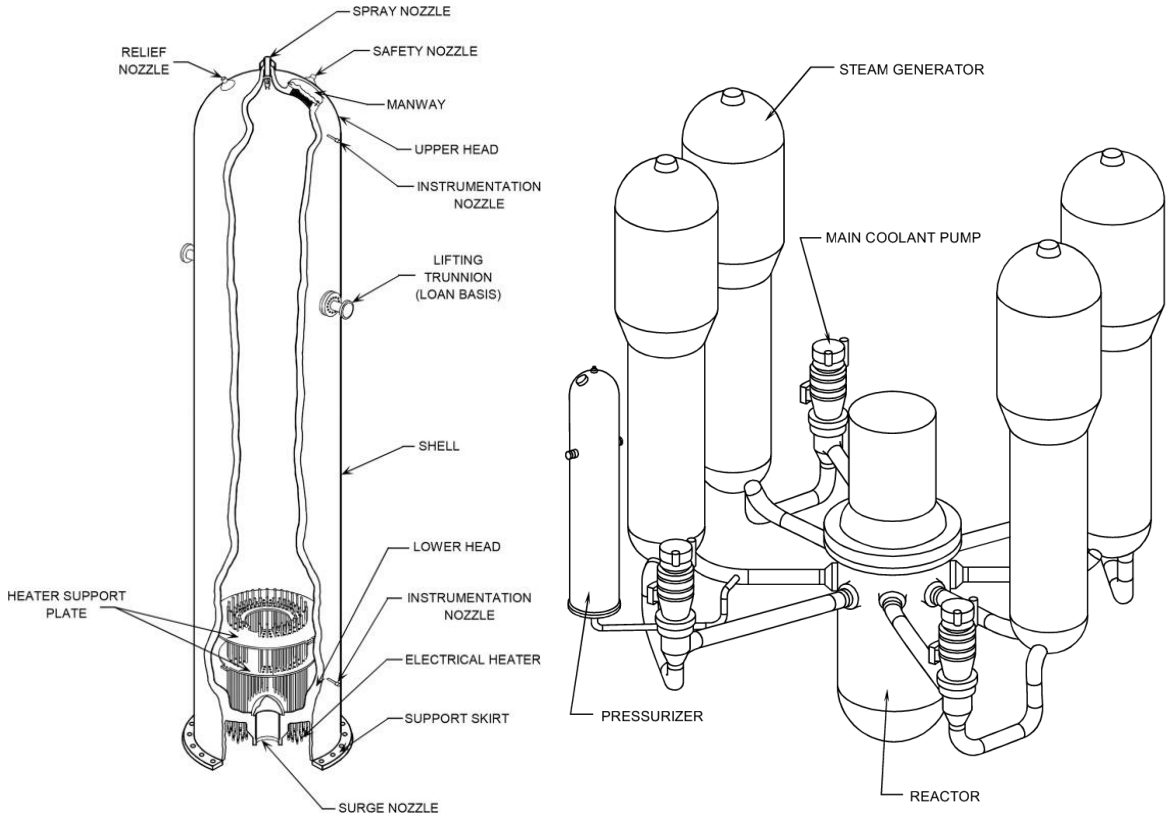

(a) (b)

Figure 4: (a) Pressurizer [9] (b) Schematic arrangement of PWR components [9]

PWR system typically contains four steam generators, four coolant pumps, and one pressurizer as shown in figure 4(b) [9]. Large PWR has four steam generators that generate steam at 293°C and 5 MPa [9]. The fuel used in PWR is cylindrical UO_2 pellets of dimensions 1 cm x 2 cm and are stacked in a 4m long stainless steel tube [9]. The expansion and contraction of pellets cause stress on the fuel tube [9]. The fuel tubes are kept under pressure by using helium at 3.4 MPa to avoid stress on the tubes and are assembled in a square pitch format called a fuel assembly which is distanced by spacers [9].

The chain reaction is controlled by control rods placed at the top of the reactor [9]. They are made up of neutron-absorbing substances which help to manipulate the multiplication factor and thereby controls the reactor [9]. In general, PWRs can give energy up to 30 MWd /kg of uranium [9].

1.2.2.2 Boiling water reactor (BWR)

In BWRs, steam is produced directly in the reactor vessel and goes to the turbines to drive the generator as shown in figure 5 [9]. It does not require special steam generators to produce steam [9]. In BWRs, water can absorb more heat and get converted to steam, unlike PWRs where water only gets heated without converting to steam [9]. This leads to less usage of water concerning time for the same power generation [9]. The pressure maintained in BWR is around 7 MPa which is half of the pressure

of PWR [9]. But, the amount of power generation per unit volume is less in BWR compare to PWR [9]. Therefore, dimensionally BWR should be bigger than PWR for the same power generation [9].

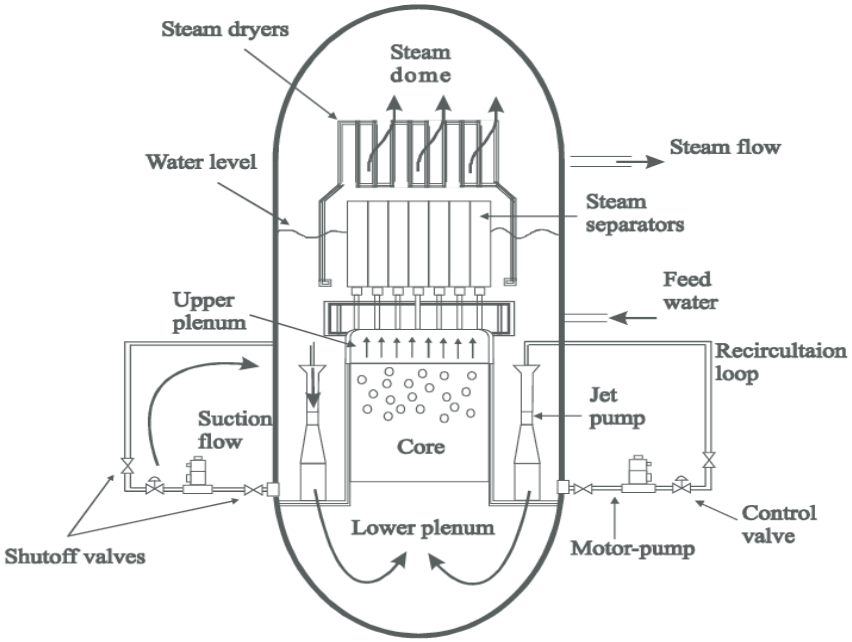

Figure 5: A typical boiling water reactor (BWR) [11]

The water gets heated due to core heat and gets converted to steam [9]. This steam is then passed through the steam separators where most of the moisture is removed and finally it then passed to the dryers which remove leftover water which then comes to the lower plenum of the reactor [9]. The jet pumps are provided to drive the reactor coolant and the fuel used in BWR is UO_2 pellets packed in tubes [9]. Unlike PWR, control rods are placed at the bottom of the reactor to control the chain reaction [9].

1.2.3 Nuclear fuel cycle

The nuclear fuel cycle is divided into two sections such as front and back end in which front end includes processes from the mining of uranium ore until loading of the fuel to a nuclear reactor and the back end of the cycle includes storage, recycling, and disposition of the nuclear fuel as shown in figure 6 [9]:

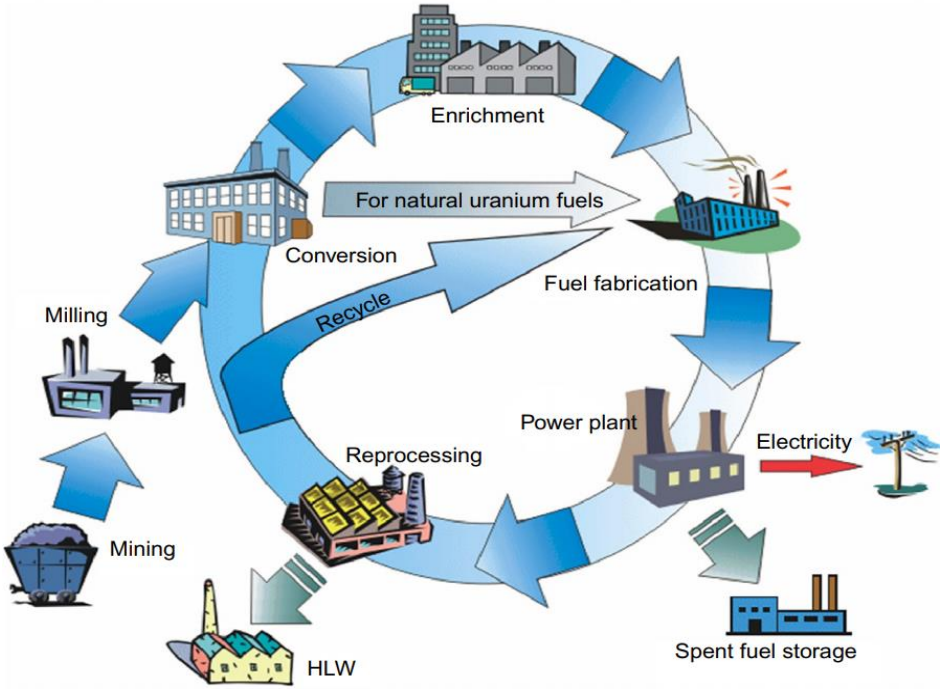

Figure 6: Nuclear fuel cycle flowsheet [12]

1.2.3.1 Front-end cycle

The uranium ore is mined, is crushed to a fine powder, and is processed to produce a concentrated solid which is called a "yellowcake" (U_3O_8) [13]. The yellowcake (U_3O_8) from milling proceeds for the conversion facility where it gets converted to uranium hexafluoride (UF_6) which has different percentages of U-234, U-235, and U-238 [13]. Natural uranium consists of about 0.7% of the U-235 which is then increased to 3-5% in the enrichment process [13]. Uranium hexafluoride is converted to the fine UO_2 powder which is further converted to cylindrical pellets and stacked in the steel tube called a fuel rod [9] [13]. Hundreds of fuel rods are combined and combined to fabricate a fuel assembly [9]. Hundreds of fuel assemblies are loaded in the nuclear reactor core and are arranged in a cylindrical manner [9].

1.2.3.2 Back-end cycle

The back-end of the fuel cycle includes the management and processing of fuel after irradiation in the reactor until its final disposition which is discussed as follows.

A] Storage of Used Nuclear Fuel (UNF)

After 12-18 months, the fuel rods are replaced with fresh fuel rods [14]. The irradiated fuel still emits a large amount of heat even after one irradiation cycle [14]. There are UNF water pools which help to cool down the fuel rods as shown in figure 7(a) [14]. UNF from commercial light water reactors is stored under 40 feet of the concrete water pool [14].

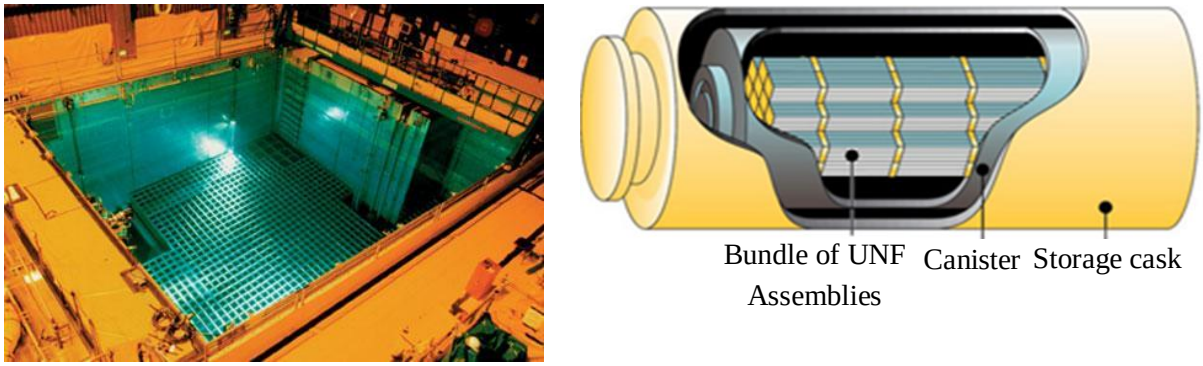

(a) (b)

Figure 7: (a) UNF water pool [14] (b) Dry cask storage [14]

UNF usually kept in spent fuel pools for five years to get sufficiently cooled and then it is shifted to dry casks which are made up of reinforced concrete where it is cooled down by natural convection – airflow [15] as shown in figure 7(b). After storage, UNF is sent to the reprocessing unit [15].

B] UNF recycling

Recycling of UNF is done to separate primarily ^{235}U from UNF. [16]. This technique also helps in the reduction of waste generation [16]. There are various separation techniques used for the recycling of used nuclear fuel [16]. The first implementation of the reprocessing technique was done in the Manhattan Project for nuclear weapons [17]. The most preferred and tried processes are aqueous reprocessing and pyro-processing [16].

I. Aqueous reprocessing

Aqueous reprocessing is the most common method use to recycle UNF which involves the separation of unused fissile material with the help of acid dissolution [16]. A typical process flowsheet is as follows:

a] Head-end process

Before aqueous reprocessing, some head-end processes are performed on fuel assemblies which include shear, voloxidation, and dissolution of fuel material into nitric acid solution [16] as shown in figure 8. The cladding around the fuel assemblies is removed and the fuel bundles containing the fuel pins are sheared and fragmented [16]. Due to the shear process, there is an emission of some radioactive and non-radioactive gases [16]. After shearing, voloxidation is done to separate tritium before recycling [16]. A nuclear fuel typically contains 94% UO_2 [16]. UO_2 is oxidized at higher temperatures such as 450 – 650°C and the product is a fine powder [16]. UO_2 reacts with oxygen and forms U_3O_8. During voloxidation, low concentrations of radioactive species are emitted [16]. This stream is comprised of contaminants such as 50% ^{14}C, 1% ^{129}I, and 5% ^{85}Kr [16].

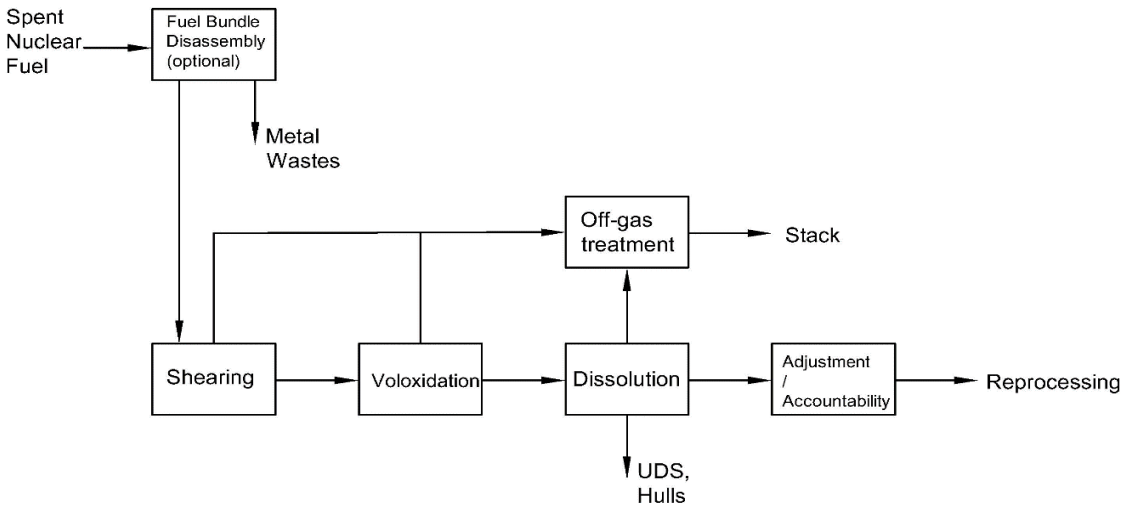

Figure 8: Head End Process [16]

b] Recycling process for UNF (PUREX)

In this process, an irradiated nuclear fuel is dissolved in an acidic solution [18] [19]. Further selective separation is done to separate uranium and plutonium [18] as shown in figure 9. Previously, the precipitation method and liquid-liquid extraction were used for the separation [18] [19]. The bismuth phosphate extraction process was first implemented in the Hanford Nuclear Reservation in 1944 to separate plutonium [18]. The continuous solvent extraction plant was then brought up at Hanford in 1952 [18]. REDOX process was also used for the separation of plutonium with methyl isobutyl ketone as an extractant [18]. PUREX process was evolved in the 1950s at General Electric's Knolls Atomic power laboratory [17]. It was scaled up in 1954 in Savannah River F Canyon and at Hanford in 1956 [16]. PUREX is the procedure that is used commercially in the world which involves liquid-liquid extraction of the UNF with the help of nitric acid, filtration of the solution, and solidification of fissile material and waste material [16] [18] [19].

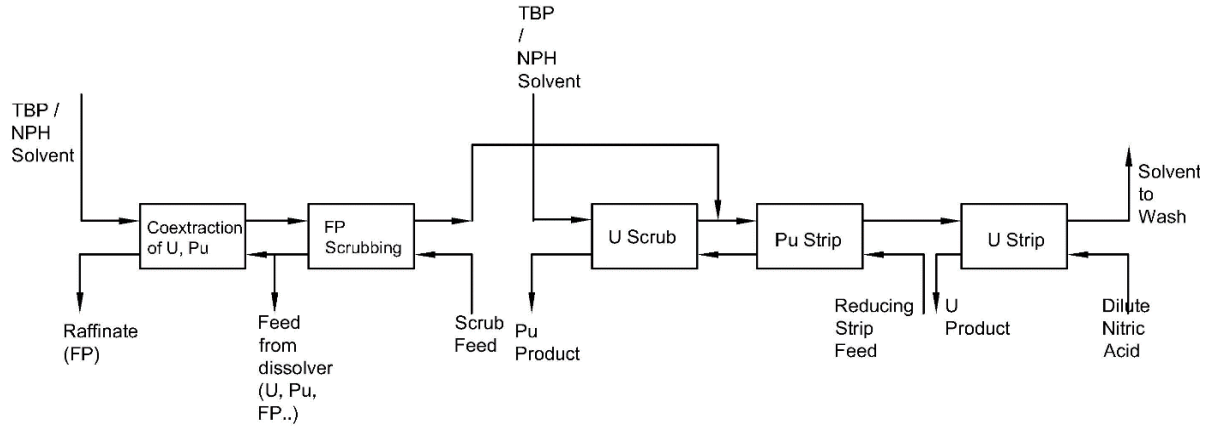

Figure 9: A schematic of a PUREX process [18]

The UNF is first dissolved in nitric acid which is then introduced to the coextraction unit [18]. TBP (tributyl phosphate) solvent is then introduced to the unit to extract U and Pu [18]. The organic phase is then sent to the FP (fission product) scrubbing section in which 0.2 M HNO_3 is introduced to scrub Zr and Ru from the solvent [18]. The solution containing Zr and Ru and the feed solution (UNF + nitric acid) enter the extraction unit [18]. The solvent enters the Pu strip unit where Pu is reduced from the tetravalent state to the trivalent state and gets extracted [18]. Typically, hydroxylamine nitrate or ferrous sulfamate is used as a reducing agent [18]. Reduced Pu strip feed enters the U scrub unit where it is introduced to the new solvent and uranium is extracted into the organic phase [18]. This organic phase with solvent is then entered into the Pu strip unit where Pu is extracted and then the solvent enters the U strip section where U is extracted into the aqueous phase using 0.01 M nitric acid at high temperature [18]. The final solution with the solvent is then washed with carbonate or hydroxide solution reverted to the extraction unit [18]. A raffinate that has no U and Pu is disposed and U and Pu products are further sent to more PUREX cycles for decontamination [18].

II. Pyro-processing

Pyro-processing is another reprocessing technique used to recycle UNF [18]. This technique uses electrochemical reactors with molten salt electrolytes for the separation of actinides with high-temperature electrorefining [17] [20]. The method is comprised of head-end processes and electrochemical processes such as oxide reduction, electrorefining, and electrowinning [21]. During oxide reduction, uranium that is in the oxidized form in the UNF is reduced to elemental form to be sent to electrorefining [21]. The reduced feed containing uranium is dissolved in eutectic salt (LiCl-KCl) and only uranium gets recovered at the cathode in the electrorefining process [21]. The molten salt containing transuranic and rare earth elements is then transferred to electrowinning using liquid cadmium cathode [21].

III. Off – gas stream from UNF recycling

Three vital off-gas streams from UNF recycling operations need to be treated: the dissolver off-gas (DOG), the vessel off-gas (VOG), and the cell off-gas (COG) [16]. The off-gas stream from the head end process is called a dissolver off-gas stream (DOG) [16]. VOG stream is comprised of an in-leakage stream from process equipment and instrument air discharged from bubblers and air sparging [16]. The cell off-gas is comprised of the off-gas from process cell ventilation [16].

C] Final disposition to waste

Spent fuel assemblies are sent for the final disposal to a permanent underground repository [16]. The United States currently does not have a repository for high-level nuclear waste [22].

1.3 Methods to capture iodine

Due to various aspects of radioactive iodine compare to other contaminants, several studies have been proposed to capture volatile and toxic radionuclides which include wet scrubbing methods and adsorption methods with different solid adsorbents [23]. Adsorption was found to be a very effective separation technique to capture volatile species [23]. Following is a review of the different studies that were being held in an effort to capture iodine species.

1.3.1 Wet scrubbing methods

Wet scrubbing methods are used to purify the air from contaminants with the help of scrubbing liquid [23] [34]. Different wet scrubbing methods have been used to capture iodine species [23] [34].

1.3.1.1 Caustic scrubbing

Caustic scrubbing is the method used to remove iodine species [23] [33] [34]. In this method, targeted gas is passed through the 1-2 M NaOH solution approximately in the packed column [23] [33]. The typical reaction occurred is as follows [23] [33] [40]:

$$3I_2\ (g) + 6\ OH^-\ (aq) \rightarrow 5\ I^-\ (aq) + IO^{3-}\ (aq) + 3\ H_2O\ (l)$$

This technique of capture is not so complicated and not expensive as well, but there is a production of radioactive liquid waste in larger volumes that need further treatment of evaporating them [23] [33]. It gives a low decontamination factor ≤ of 100 [23] [33]. The decontamination factor is the ratio of radioactive iodine at the inlet and the outlet.

1.3.1.2 Mercurex

In this process, 0.4 M $Hg(NO_3)_2$ and 14 M HNO_3 solution is circulated in a column [23] [33]. This process can be used to remove both organic and inorganic iodine species [23] [33]. The process involves mercury, which is the disadvantage of this process [23] [33].

Inorganic Iodide capture [23] [33] [40]:

$$6I_2 + 6\ Hg(NO_3)_2 + 6\ H_2O \leftrightarrow 5\ HgI_2 + Hg(IO_3)_2 + 12\ HNO_3$$

Organic iodide capture [23] [33] [40]:

$$2CH_3I + Hg(NO_3)_2 \leftrightarrow HgI_2 + 2CH_3NO_3$$

$$CH_3I + Hg(NO_3)_2 \leftrightarrow HgI^+ + CH_3NO_3 + NO_3^-$$

It requires Hg in large quantities which is poisonous [23] [33].

1.3.1.3 Iodox

In this process, 20-23 M HNO_3 is used as a scrubbing solution [23] [33]. HI_3O_8 can be acquired by evaporation of nitric acid which gives a favorable platform for waste forms [23] [33]. This process is expensive and requires special chemical resistant equipment [23] [33]. The reactions along with this process are as follows [23] [33] [40]:

$$2CH_3I + 4HNO_3 \leftrightarrow 2CH_3NO_3 + I_2 + N_2O_4 + 2H_2O$$

$$I_2 + 4\ HNO_3 \leftrightarrow 2I^+ + 2NO^{3-} + N_2O_4 + 2H_2O$$

$$I^+ + 3\ HNO_3 + NO^{3-} \leftrightarrow IO^{3-} + H^+ + 2N_2O_4 + 2H_2O$$

1.3.1.4 Electrolytic scrubbing

It involves the use of ≈ 1M Co^{3+} in 8-12 M HNO_3 in which Co^{3+} oxidizes iodine to non-volatile form and the product is $Co(NO_3)_2$ and $Co(IO_4)_2$ [23] [33] [40]. This method has good control over occurring redox reactions and on the evolution of new iodine species [23] [33] [40]. But the byproducts formed do not give a suitable platform to convert into waste easily [23] [33] [40].

1.3.1.5 Fluorocarbon solvents

Dichlorodifluoromethane (R-12) is loaded in the packed column and operated at 300 psig and for the temperature range of -25 to 10°F [23]. This method is useful to capture elemental as well as volatile organic iodine species with a decontamination factor greater than 10^4 [23]. The presence of other species such as NO_2 does not affect the solvent or the process. [23].

1.3.1.6 Silicone-organic (polymethyl siloxane) solvents

The silicone-organic solvents are found as good for the capture of elemental iodine with the decontamination factor of 150 [23]. These solvents do not get affected by NO_2 [23].

1.3.2 Adsorption methods using porous solid adsorbents

Several studies have focused on the adsorption phenomenon for capturing iodine species. A myriad of solid adsorbents was used to capture which are listed as follows:

1.3.2.1 Activated carbon

Activated carbon has been used for the capture of gaseous phase iodine [23] [35]. It exhibits good performance but has a low capture ability at higher temperatures [23] [35]. It does not possess good resistance regarding the contaminants such as NO_X [23] [35]. Activated carbon impregnated with TEDA and KI exhibits good performance and gives a decontamination factor up to 10^4 [33] [40].

1.3.2.2 Macroreticular resins

Macroreticular resins are functionalized acrylic esters [23]. They possess excellent affinity towards iodine with good resistance regarding the contaminants such as NO_X [23]. The resins are porous and acid-resistant but do not exhibit a good capture ability over 50°C [23].

1.3.2.3 Silver-loaded adsorbents

Silver-loaded adsorbents include silver-exchanged zeolites or silver-loaded materials [23] [36]. They show excellent adsorption capacities for elemental as well as organic iodine capture [23] [36] [37].

A] Silver nitrate loaded sorbents

Silver nitrate loaded sorbents exhibit good performance in the capture of elemental as well as volatile organic iodine species [23]. The iodine on reaction with silver nitrate forms a stable complex of silver iodide or silver iodate [36]. Silver nitrate impregnated silica and alumina have been tried for iodine capture [23]. Silver nitrate loaded with silicic acid called AC-6120 claimed the capture efficiency of around 99% with a silver content of 8-12% [23]. Silver nitrate loaded alumina (AgA) claims the same efficiency with a silver content of 24% [23]. Silver nitrate loaded adsorbents are economic and exhibit good capture ability even in the presence of contaminants and at elevated temperatures [23]. But, the capture ability is reduced by high moisture content and organic species [23].

B] Silver functionalized silica aerogels

Silver functionalized silica aerogels possess high porosity and have the ability to become hard after iodine capture and form a silica-based product with AgI complex [42]. They possess a good affinity towards iodine species and are stable as well [42]. They have a good iodine loading capacity of around 48 wt.% [42].

C] Ag exchanged zeolites

Metal exchanged ceramics use a metal that has a strong affinity towards iodine [23]. Cd, Cu, Hg, Mn, Pb, Pd, Ag, and Tl have been used for capturing iodine species [23]. But Ag is more efficient among all because it chemisorbs iodine species and makes a stable complex AgI [36] [38]. It is found as the most stable adsorbent in a capture [36]. Ceramics such as Al_2O_3 (AgA), SiO_2 (AgS) and Ag loaded zeolite includes AgZ (mordenite), faujasite (AgX) have coatings or are impregnated with $AgNO_3$ [23]. A typical reaction is as follows [23]:

$$3I_2\,(g) + 6AgNO_3\,(s) \rightarrow 4AgI\,(s) + 2AgIO_3\,(s) + 6NO_2(g)$$

$$CH_3I\,(g) + AgNO_3\,(s) \rightarrow CH_3NO_3\,(g) + AgI\,(s)$$

$$I_2\,(g) + 2Ag\,(s) \rightarrow 2AgI\,(s)$$

$$2CH_3I\,(g) + 2H_2O\,(g) + 2Ag\,(s) \rightarrow 2AgI\,(s) + 2CH_3OH\,(g) + H_2\,(g)$$

Recent studies have focused on silver exchanged zeolites [23] [33]. Silver exchanged zeolites are stable adsorbents [36]. They also have a porous structure and a surface area ranging from 400-450 m^2/g [30] [37]. They have an average loading of 100 to 130 mg I_2/g Ag-MOR [30] [37]. Mordenite is a zeolite mineral [30] [37]. Silver mordenite does not require higher temperatures for capture [30] [37]. The recycling ability of silver mordenite is high and it can be recycled 13 times with a 20% decrease in adsorption capacity [30] [37]. It is also acid-resistant due to high Si/Al ratio [30] [37].

Ag-ZSM-5 (7.2wt% Ag) is used as an adsorbent to capture volatile methyl iodide for a temperature range of 50 – 150°C [39]. The feed concentration of 2000 ppm was introduced to the adsorbent for 200 minutes [39]. It was found as, at lower temperatures, Ag-ZSM-5 has a higher capacity

than at higher temperatures as can be seen from the following numbers: 112, 98, 79, 68, and 54 mg/g Ag-ZSM-5 at 50, 70, 90,120 and 150°C, respectively [39].

Methyl iodide adsorption studies were performed on silver-exchanged faujasite zeolite (Si/Al = 2.5) as well [38]. Methyl iodide concentration at the adsorption column inlet was 1333 ppm and the temperature was maintained at 100°C [38]. It was reported that the breakthrough happened in 66 minutes [38]. This zeolite adsorbent adsorbed 209 mg/g CH_3I with 23 wt.% silver content [38].

The adsorption behavior with silver ion-exchanged zeolite, zeocarbon, and activated carbon as an adsorbent was also tested as shown in table 1 [41]. Different temperatures were tried to determine the behavior of the adsorbents as shown in table 1 [41].

Table 1: Adsorption capacities of different adsorbents

Type of an adsorbent	**Temperature (°C)**	**The amount adsorbed (mg/g)**
Activated carbon (AC)	30	283.65
	170	8.79
13X	30	43.09
	100	109.42
	170	164.53
	250	64.84
	380	37.17
AgX - 10 Wt%	100	182.54
	170	172.11
	250	158.39
	380	128.77
AgX - 20 Wt%	100	219.6
	170	209.26
	250	194
	380	170.77
AgX - 30 Wt%	100	252.22
	170	238.13
	250	226.17
	380	192.55
Zeocarbon (ZC)	30	147.82

It was found as the lower weight percent silver mordenite is more efficient in the sense of silver utilization as shown in table 2 [41].

Table 2: Silver utilization scenario

Temperature (°C)	Wt.%	Silver utilization %
170	10	100
	20	84
	30	68
250	10	98
	20	75
	30	63
380	10	67
	20	57
	30	45

1.3.2.4 Chalocogen-based aerogels

Chalcogen-based aerogels possess good iodine capture ability as reported by Riley et al [40] [43]. Loading capacity up to 225% was found for sulfidic chalcogels, which was attributed to both due to chemisorption of species and physisorption as well due to the high surface area of the adsorbent [43].

1.3.2.5 Metal-organic framework (MOF)

Metal-organic frameworks are crystalline in nature in which metal ions are linked with organic ligands [44]. They have a very high surface area of around 10^4 m^2/g and possess a high affinity towards I_2 [33]. They have a highly porous and flexible structure with low thermal stability [33].

1.4 Summary

Among the different off-gas streams, vessel off-gas stream is typically comprised of volatile radionuclides that are difficult to capture. Several porous sorbents have been studied for the capture of volatile organic iodine species. Among them, silver-loaded mordenites were found as more efficient over other sorbents, and taking into consideration its scope towards iodine capture, it was decided to do an extensive investigation of mordenites to study their behavior of capture. The sorbents' response towards capture was studied in which very low concentrations of volatile organic species such as methyl iodide were used to simulate actual vessel off-gas conditions as described in the following chapters.

Chapter 2: Materials and Methods

Recent studies have indicated silver mordenite to an effective adsorbent for the capture of iodine species as discussed in chapter 1. The adsorbents used in this study are based on mordenite and the effect of silver content in mordenites is studied by varying from 0-100% of cations in the zeolite structure.

2.1 Materials

A commercially available zeolite mordenite, sodium (Fisher Scientific: catalog no. AA4587622) was used as the base adsorbent. Partially and fully exchanged silver mordenite were synthesized in house to compare the effect of silver on adsorption. Both sodium and silver cations are present in partially exchanged silver mordenite while all the sodium ions are replaced by silver ions in fully exchanged silver mordenite.

2.2 Synthesis of silver mordenites

Partially and fully exchanged silver mordenite were synthesized using the procedure described below:

2.2.1 Preparation of the adsorbents

A two-step procedure comprised of preparation of silver nitrate solution and cation exchange procedure which involves sodium – silver ion exchange was employed to synthesize silver mordenites. Silver nitrate solution was prepared first by dissolving $AgNO_3$ (Fisher Scientific: catalog no. AA1141414) powder in DI water. For the cation exchange step, sodium mordenite powder was dried at 110°C in an oven for two hours and then contacted with the $AgNO_3$ solution. The reaction can be written as,

$$NaMOR\ (s) + Ag^+\ (aq.) + NO_3^-\ (aq.) \rightarrow AgMOR\ (s) + Na^+\ (aq.) + NO_3^-\ (aq.)$$

The contents of the vessel were refluxed for 2 hours maintaining the temperature at 90°C as shown in figure 10.

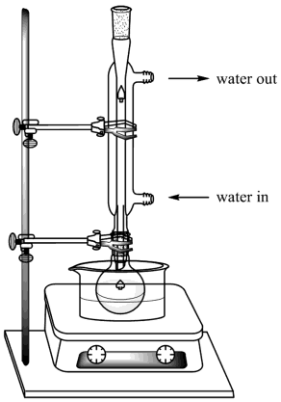

Figure 10: Reflux setup [24]

Sodium ions from sodium mordenite get exchanged with silver ions from an aqueous solution of $AgNO_3$ as described in the reaction earlier. The suspension after contact was filtered using a Buchner funnel and rinsed with 1.5 to 2 liters of DI water. The filtered solid was air-dried first and later in an oven at 120^0 C for several hours. Obtained mordenite was a very fine powder which was then stored in the desiccator to avoid absorption of moisture. Partially and fully exchanged silver mordenite were prepared by varying the concentration and volume of $AgNO_3$ and amount of NaMOR as shown in table 3.

The percent exchange is the ratio of silver moles exchanged over the available sodium moles for exchange. A Mohr's titration in a reverse manner was performed after the synthesis of the adsorbent to verify the actual percent exchange of the adsorbents. 0.0005 M NaCl was titrated against $AgNO_3$ ($AgNO_3$ solution of unknown molarity obtained after exchange). Potassium chromate (0.025M) was used as an indicator. By using the formula, $M_1 \times V_1 = M_2 \times V_2$, the unknown molarity of $AgNO_3$ was determined followed by actual percent exchange, Ag-Na ions.

Table 3: Adsorbent preparation measurements

Molarity of $AgNO_3$ (M)	**Amount of NaMOR taken (g)**	**The volume of the solution (L)**	**Actual percent exchange**	**Amount synthesized (g)**
0.005	20	0.4	3.8	20.17
0.05	15	0.6	63	17.09
0.1	15	0.6	100	18.32

2.2.2 Pelletization of the adsorbent

The adsorbent powder was first dried to remove absorbed moisture if any and then the pellets were made with the help of a manual pellet press as shown in figure 11. The press setup comprises of three plates visually a base plate, a plate with holes, and a plate with thin pins.

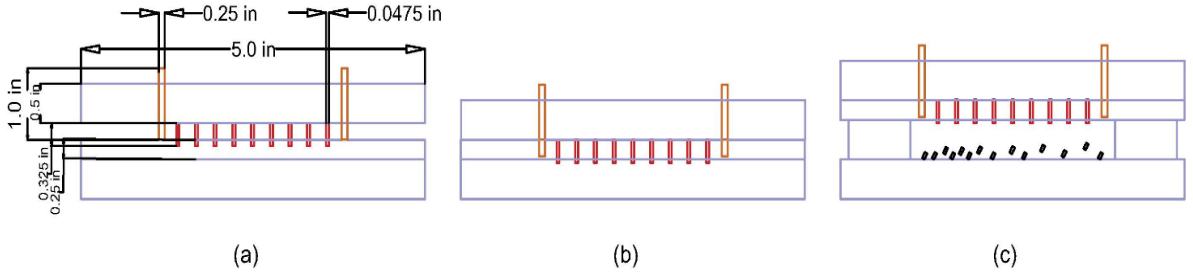

Figure 11: The pellet press

The powder was filled into the holes of one of the plates, which is supported on the base plate. The third plate having matching pins was overlaid on the plate with holes and pressure applied to compact the powder inside the plate with the help of an arbor press. After compaction the powder inside the plate, pellets were released out by removing the base plate and forcing the pins through the holes.

2.3 Experimental instruments, setups, and procedures

There were various sets of experiments performed to test different parameters such as the material of construction, temperature, and silver effect on the ability of the adsorbent to capture. Experimental assembly and corresponding instruments are discussed as follows.

2.3.1 Experimental instruments

Various instruments were used to execute the dynamic adsorption experiments which are as follows :

2.3.1.1 Permeation tube system

The permeation tube system (VICI Metronics Inc. DYNACALIBRATOR MODEL 230) was used in the adsorption studies as an iodine species generator as shown in figure 12. It can create concentrations from ppb to ppm-level. The methyl iodide permeation tube (methyl iodide permeation tube VICI Dynacalibrator, PD-4600-U35) was placed inside the system. The air served as a carrier gas. By varying the temperature of the permeation chamber and air flow rate, the desired concentration was achieved.

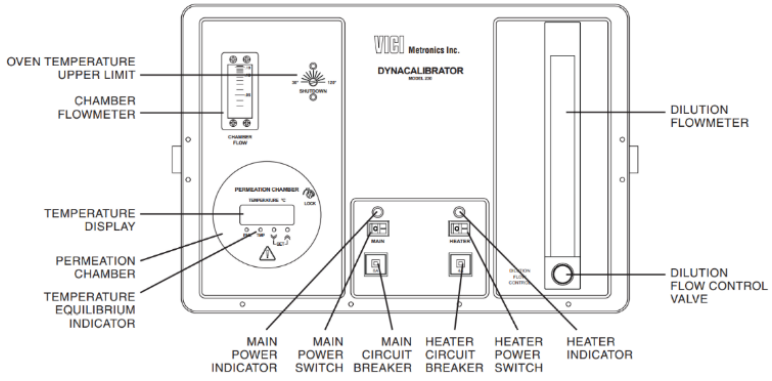

(a)

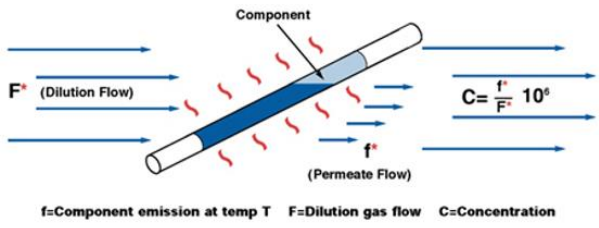

(b)

Figure 12: (a) Front panel of Dynacalibrator [27] (b) Permeation tube [28]

2.3.1.2 Analysis setup

The analysis setup included GC-ECD (SRI 8610C GC with a 6 ft Restek Hayesep Q 1/8" OD packed column) which was used to monitor the feed and concentrations after adsorption. Taking into consideration the generation of ppb level iodine species, an electron capture detector which is sensitive towards halogenated hydrocarbons was used to measure the low concentrations. Six port sampling and valve switching assembly were used to collect the sample and detection of it as shown in figure 13. The column temperature was maintained at 150°C with the ECD temperature maintained at 250°C and the standing current was 300 pA. The GC-ECD was calibrated using a 1 ppm methyl iodide gas cylinder balanced with nitrogen.

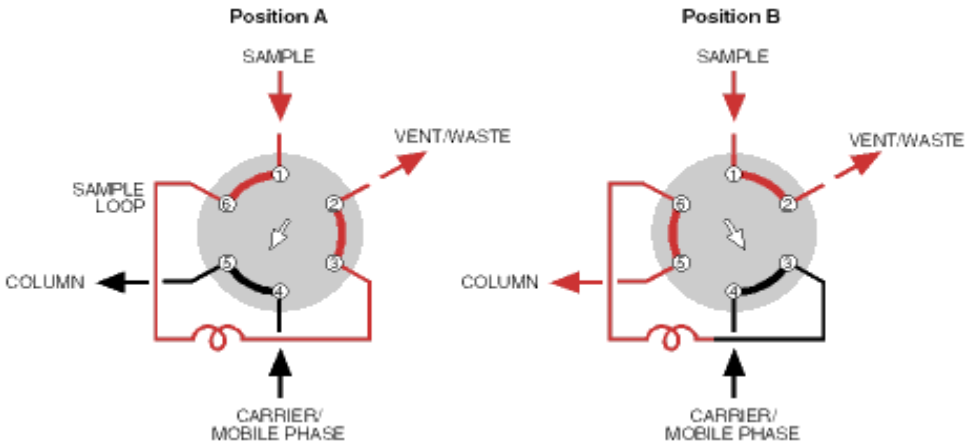

Figure 13: Six port sampling setup [29]

Position A: The sample comes in and fills the sample loop. Meanwhile, the carrier gas flows through the column.

Position B: The carrier gas enters the sample loop and takes the sample to the column for detection.

2.3.2 Experimental setup 1

This experiment served as the preliminary setup to observe the adsorbent's behavior. The adsorbent pre-treatment and setups are discussed as follows.

2.3.2.1 Packing of the column

The glass column of dimensions 4 in height and 1 in diameter was used for this experiment. The packing configuration of the sorbent is as shown in figure 14.

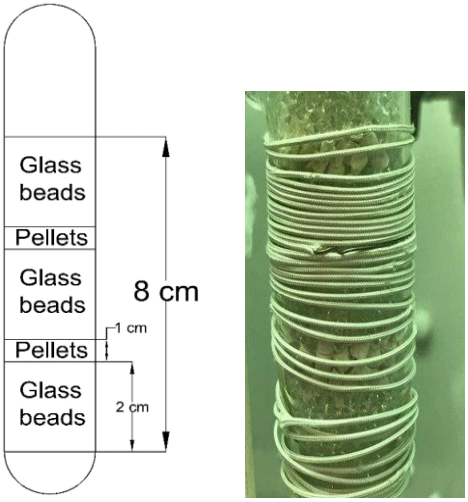

Figure 14: A packed column

The packing of the column with the pellets followed by glass beads allows a good distribution of a gas flow. The adsorption column was packed with sodium mordenite for run 1 and 3.8% exchanged silver mordenite for run 2. For the first run of an experiment, the column was packed with cylindrical pellets of dimensions 3mm x 3mm approximately. There were 72 pellets in the adsorption column. The rest of the column was packed with glass beads. The column was packed with different layers. There were 3 layers of glass beads with a thickness of 2cm each. There were 2 layers of pellets of thickness 1cm each. There were 36 pellets in each of the two stages. These layers are there in the column in an alternate fashion. The column temperature typically was 200^0C.

2.3.2.2 Activation / Pre-treatment of sorbent

It was reported that silver in a metallic state has good adsorption capacity [30] [31]. Therefore, partially exchanged silver mordenite and fully exchanged silver mordenite were pre-treated with hydrogen. The adsorbent was loaded into the column as shown in figure 14 and 4% H_2 + 96% Ar was blended and passed through the adsorption column for 24 hrs. at 500^0 C at the flow rate of 360 ml/min as shown in figure 15.

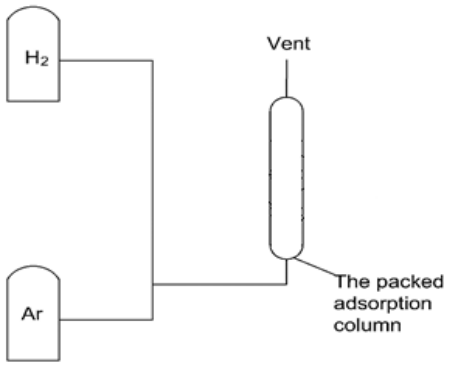

Figure 15: Activation of the adsorbents

The typical activation reactions could be as follows,

For partially exchanged silver mordenite,

$$2\ (\text{Na-AgMOR})\ (s) + H_2\,(g) \rightarrow 2Ag^{\circ}\ (s) + 2(\text{H-Na})\text{-MOR}\ (s)$$

For fully exchanged silver mordenite,

$$2\ \text{AgMOR}(s) + H_2\,(g) \rightarrow 2Ag^{\circ}(s) + 2\text{H-MOR}(s)$$

2.3.2.3 Working and construction

The experimental setup consists of an adsorption column, an iodine species generator (permeation tube system), and an analysis setup. An adsorption column was packed with the sorbent. The adsorption column used was non-jacketed and an electrical heating coil was wrapped around the column to obtain desired temperatures. The column with the heating coil was surrounded by fiberglass insulation to minimize heat losses. The typical piping and instrumentation are shown in figure 16.

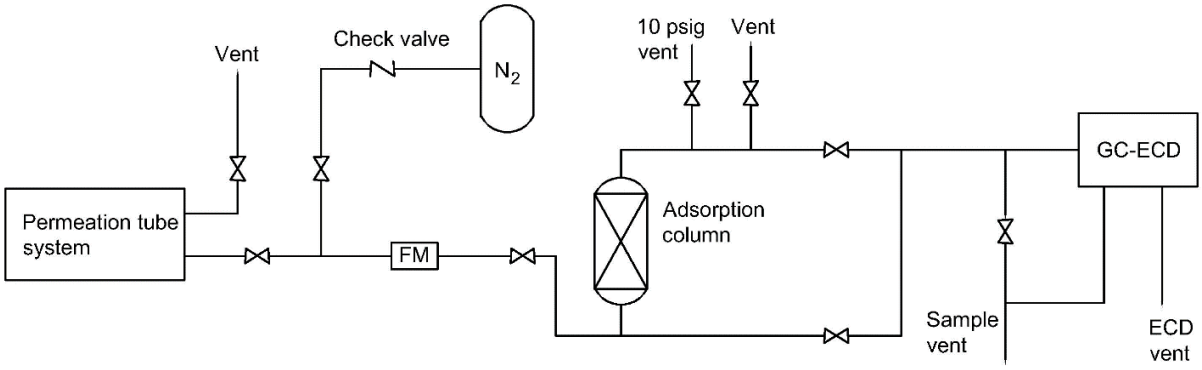

Figure 16: Experimental setup

FM – flow meter, GC-ECD – gas chromatography-electron capture detector

Low concentrations (100-150 ppb) of methyl iodide were passed through the adsorption column. There was a flow meter (FM) to read the flow rate through the column. A thermocouple was provided to monitor the column temperature. There was a pressure regulatory valve (cracking pressure 10 psig) to avoid the hazard of excess pressure load on the column. There was a nitrogen supply connection to flush the whole setup in case there is residual accumulated to avoid incorrect concentration detection.

Adsorbents used in these studies were sodium mordenite and silver mordenite (3.8% exchanged). 3.45 grams of sorbents were loaded in the column according to the expected breakthrough time. The flow rate was maintained at 1.0 L/min at the inlet of the column and the temperature was maintained at 200°C. The whole experimental setup was inside the fume hood.

2.3.3 Experimental setup 2

The experiment is designed to compare the different adsorbents' behavior in a SS column with identical conditions and the effect of silver content from 0 to 100% silver in the adsorbent. Three different columns were operated simultaneously to ascertain their behavior. The packing style, activation, and experimental setup are discussed as follows.

2.3.3.1 The packing of a column

For the second run of an experiment, the column was packed in a different style. SS316 tube of 0.4 in ID was used as the adsorption column.

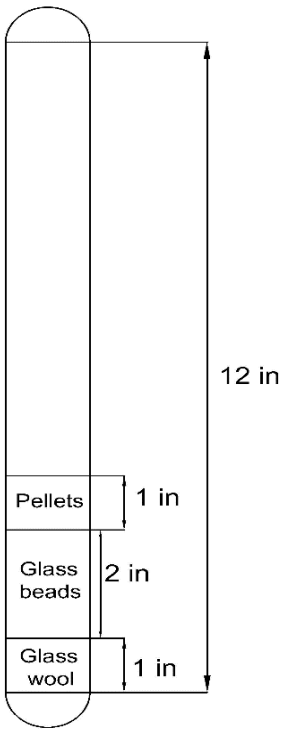

Figure 17: The packing of the column

All three columns were packed in the same fashion as shown in figure 17. The columns were packed such that there will be a uniform platform for the pellets. At the bottom, there was approximately 1 in thick layer of glass wool insulation. There was a 2 in. layer of glass beads resting on top of it which helped to get the plain platform for the adsorbent pellets. The adsorbent pellets were loaded on top of the layer of a glass bead. The sorbent was pre-treated with hydrogen at 400°C, 24 hours at a flow rate of 360 ml/min like in experiment setup 1.

2.3.3.2 Working and construction

This experimental system, consists of three adsorption columns were made up of stainless steel (SS316 grade) which are packed with different adsorbents that included sodium mordenite (NaMOR),

partially exchanged (63%) silver mordenite (Na-AgMOR), and fully exchanged silver mordenite (AgMOR) in column 1, column 2 and column 3 respectively as shown in figure 18. The current setup has the provision to monitor the inlet and outlet concentration of all three columns by manual operation. The iodine species generator system and the analysis setup were the same as used for the glass column adsorption experiment. Low concentrations (100-150 ppb) of methyl iodide were passed through the adsorption column. There was a thermal mass flow meter (0-5 SLPM) to measure the outlet flow rate through the column. Thermocouples were provided to monitor the column temperatures. There was a pressure regulatory valve to avoid the hazard of excess pressure load on the column. The flow coming out from the permeation tube system was 3.8 L/min before splitting. The flow of 3.0 L/min was then split into three streams to get the same flow rate of 1 L/min through each of the three columns and the remaining 0.8 L/min was vented off. There were needle valves at the inlets of column 2 and column 3. They were adjusted to provide a flow rate of 1 L/min through column 2 and column 3. Consequently, the flow through column 1 was also 1 L/min. There is another flow meter (ranged 0- 5 SLPM manufactured by Teledyne Hastings) before the splitting of the flows who read the flow at the permeation tube system outlet. FM 1 and FM 2 are flow meters that read flow rates at the inlet and column outlet flow rates.

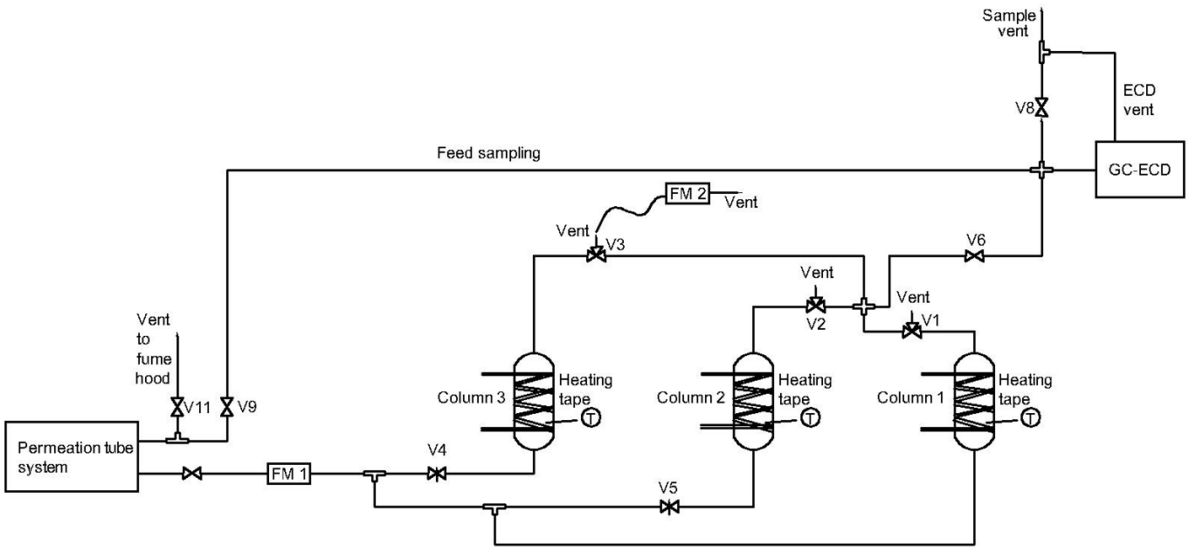

Figure 18: Piping and instrumentation

There was a three-way valve at the outlet of each column. The valve directed the flow to vent during normal operation. For the column outlet sampling, the valve position was shifted towards the GC inlet. The other two columns' valve position was towards the vent at the same time. The vent of the permeation tube system was the same as the column inlet. Therefore, to determine inlet concentration, the concentration of the vent stream from the permeation tube system was determined to avoid

disturbance to the columns. Valve v11 is shut off and valve v9 is opened to direct the flow through the GC-ECD for determining the concentration in the inlet stream. The temperature of 170°C was maintained for all the columns.

1.0 gram of sorbents were loaded in the column according to the expected breakthrough time. The inlet concentration of 140 ppb was passed through the columns and the columns outlet concentration behavior was monitored which is discussed in the next chapter 3.

Chapter 3: Experimental analysis

In this chapter, experimental results are discussed to investigate the adsorption behaviors of used mordenites in different environments. To illustrate this, breakthrough predictions, adsorption capacities, and adsorption-desorption cycles are discussed.

3.1 Experimental results and discussion

The adsorption experiments performed on different mordenites and with different material of construction are summarized as below:

3.1.1 Experimental setup 1

Breakthrough predictions were made to estimate the adsorbent ideal exhaustion time. The breakthrough is the state where the outlet concentration becomes equal to the inlet concentration of the adsorption column. None of the adsorbents has achieved a breakthrough as shown in figures 19 and 20.

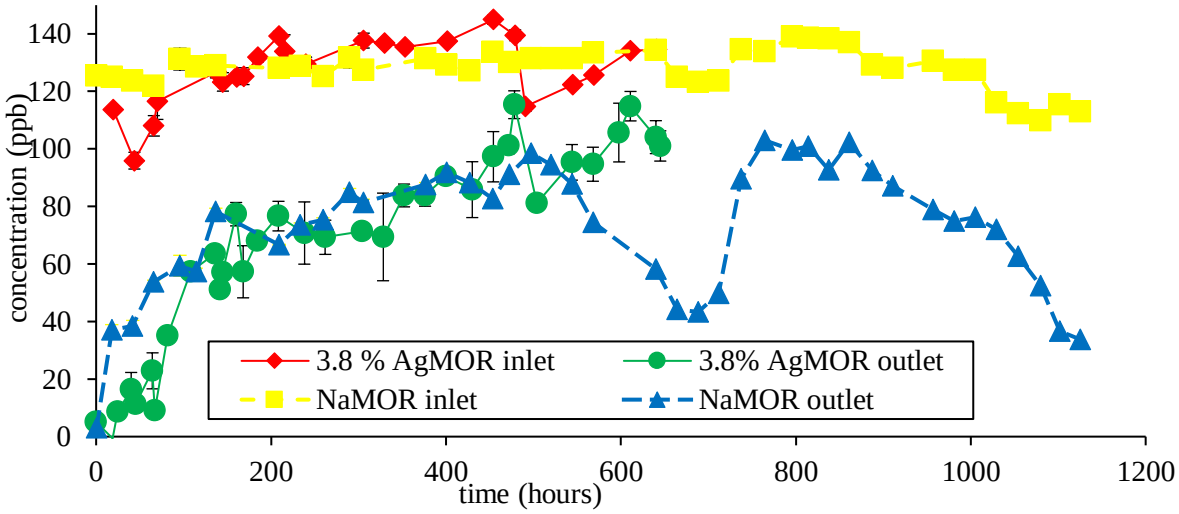

Figure 19: Breakthrough plot for experiment setup 1

The adsorption experiment run for sodium mordenite as an adsorbent was performed in a glass column. The run time for the experiment was around 7 weeks. The amount adsorbed during the run time was found as 6.76 mg CH_3I/g of NaMOR. Inlet concentration was around 140 ppb and outlet concentration was around 100 ppb with no column breakthrough. For 3.8% exchanged silver mordenite, the run time for the experiment was around 7 weeks. The amount adsorbed during the run time was found as 5.58 mg CH_3I/g of Na-AgMOR. The same inlet concentration of 140 ppb was maintained throughout the experiment.

3.1.2 Experimental setup 2

In this experimental run, different mordenites such as sodium mordenite, 63% exchanged silver mordenite, and fully exchanged silver mordenite were loaded in different SS316 columns and the adsorption was performed simultaneously. The results are discussed as below:

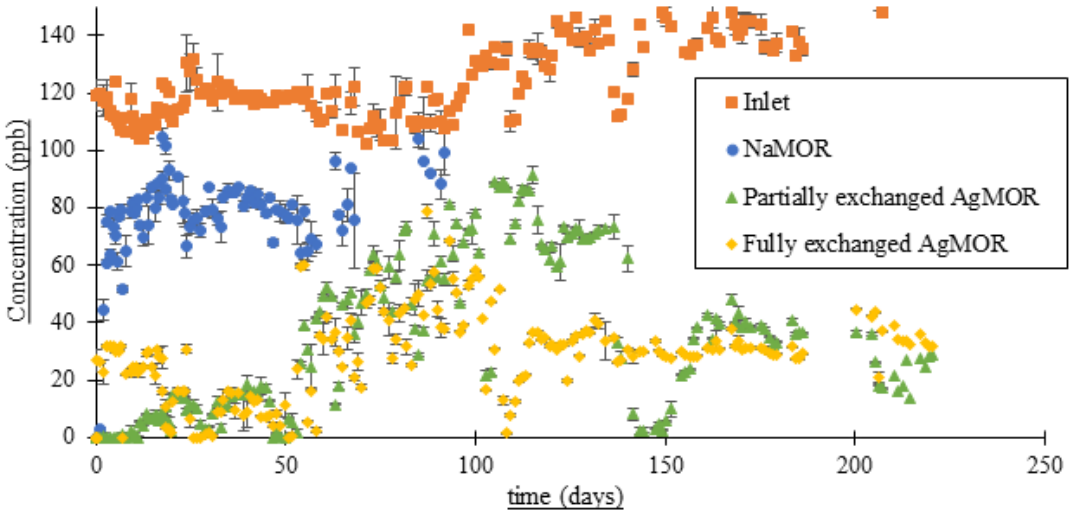

Figure 20: Breakthrough plot for experiment setup 2

Inlet concentration was maintained around 120 ppb for each of the columns. The run time for the sodium mordenite experiment was around 6 weeks and the amount adsorbed during the run time was found as 20.29 mg CH_3I/g of NaMOR. The run time for 63% exchanged silver mordenite experiment was around 31.4 weeks. The amount adsorbed during the run time was found as 168.7 mg CH_3I/g of Na-AgMOR. The experimental run time for fully exchanged silver mordenite as an adsorbent was around 31.4 weeks. The amount adsorbed during the run time was found as 215 mg CH_3I/g of AgMOR.

3.1.3 Summarized experimental results

In the case of the silver mordenite, the iodine forms a stable AgI complex when reacts with silver within the adsorbent [31] [32] [33]. Assuming all the present silver in partially and fully exchanged silver mordenite will adsorb iodine species, breakthrough time was predicted as shown in table 4.

Table 4: Experimental results

Adsorbent	**MOC of the column**	**Run time (weeks)**	**The amount adsorbed (mg CH_3I/g adsorbent)**	**Expected breakthrough (weeks)**
NaMOR	Glass	7	6.76	N/A
	SS316	6	20.29	
3.8% AgMOR	Glass	7	5.58	10.42
63% AgMOR	SS316	31.4	168.7	24.7
100% AgMOR	SS316	31.4	215	36.4

It was found as sodium mordenite has more iodine loading in the SS316 column compared to the glass column. Not much difference was found between the capacities of sodium mordenite and 3.8% AgMOR in the glass column. It was found that 63% exchanged and fully exchanged silver mordenite in the SS316 column had a considerable amount of loading with no exhaustion.

3.2 Adsorption – Desorption Cycles for sodium mordenite with different materials of construction of column

It was found that sodium mordenite favors physical adsorption of iodine species over chemical adsorption compare to silver loaded mordenites [37]. To verify this, various adsorption-desorption cycles were performed at different temperatures and using different materials of the construction column which is discussed as follows.

3.2.1 Procedure

Adsorption-desorption cycles were performed for the sodium mordenite sorbent at different temperatures: 25°C, 70°C, 120°C, and 170°C Three adsorption-desorption runs were performed at each temperature.

3.2.1.1 Adsorption

Fresh 1.0 g of the adsorbent pellets, here, sodium mordenite, were packed in the column. The arrangement is such that, methyl iodide of concentration around 120 ppb with air as a carrier gas was passed through the adsorption column in an attempt to saturate the sorbent with methyl iodide. The flow rate was 0.5 L/min through the column for the adsorption.

3.2.1.2 Desorption

To remove the physisorbed methyl iodide, the desorption has been done. Methyl iodide flow was stopped and just air was passed through the column at the flow rate of 0.43 L/min for desorption. The air was passed until no methyl iodide was detected at the column outlet.

3.2.2 Calculations:

Based on the adsorption and desorption plots, the amount adsorbed and desorbed values were calculated.

A typical calculation procedure is as follows:

For the amount adsorbed calculations, inlet concentrations and column outlet concentrations were plotted as well. The area between the two curves was calculated to get the amount adsorbed. For the amount desorbed calculations, the area below the outlet concentration was taken.

3.2.2.1 Area

$$\text{Area} = \text{ppb} \times \text{hours}$$

3.2.2.2 No. of moles

$$\text{No. of moles} = \frac{\text{Area(ppb x hours)x flowrate } \left(\frac{\text{L}}{\text{h}}\right)\text{x } 0.000000001 \text{ xP (atm)}}{\text{R}\left(\frac{\text{L x atm}}{\text{mol x K}}\right) x\ T\ (K)} = \text{moles}$$

3.2.2.3 Amount adsorbed

$$\text{Amount adsorbed} = \text{moles x } 141.94 \text{ x } 1000 = \text{mg } CH_3I$$

3.2.2.4 Amount adsorbed (mg/g)

$$\text{Amount loaded} = 1.0178 \text{ g}$$

$$\therefore \text{ amount adsorbed mg/g} = \frac{Amount\ adsorbed}{1.0178} = \text{mg } CH_3I\text{/g of NaMOR}$$

3.2.3 Observations

Three cycles of adsorption-desorption were performed for the adsorbent (sodium mordenite) in SS316 column and FEPE made column to see the effect of material of construction and temperature on adsorption mechanism which is discussed as follows.

3.2.3.1 SS316 column

The SS316 grade column was used for the adsorption-desorption cycles at different temperatures which are discussed as follows.

A] Adsorption on glass beads

As a control run, glass beads were packed in the column to see their behavior towards methyl iodide species which is discussed here. A set of four temperatures were tried such as 25, 70, 120, and 170°C. About 120 ppb of methyl iodide with air was passed through glass beads and the column outlet concentrations were monitored.

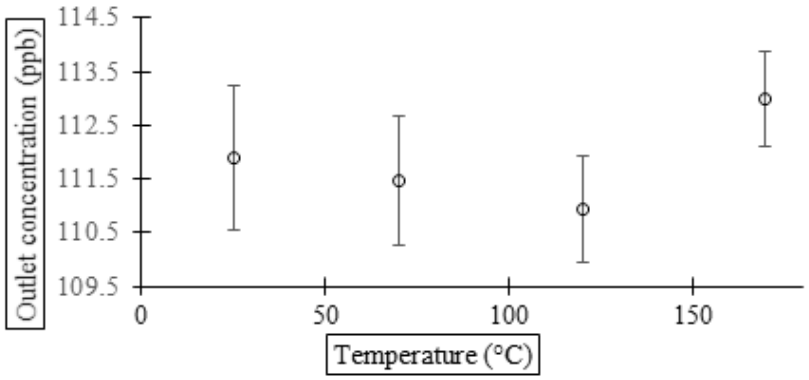

Figure 21: Outlet concentration (ppb) vs temperature (°C)

The column outlet concentration did not show any change with different temperatures as shown in figure 21 which is almost the same as feed concentration.

B] Adsorption–desorption cycles at 25°C

The findings from the performed adsorption-desorption cycles at 25°C are discussed as follows.

I. Adsorption

Three adsorption cycles followed by desorption cycles have been performed as shown in figure 22. The average amount adsorbed is 8.17 µg/g. The time required for the adsorption was nearly 2.5 hours.

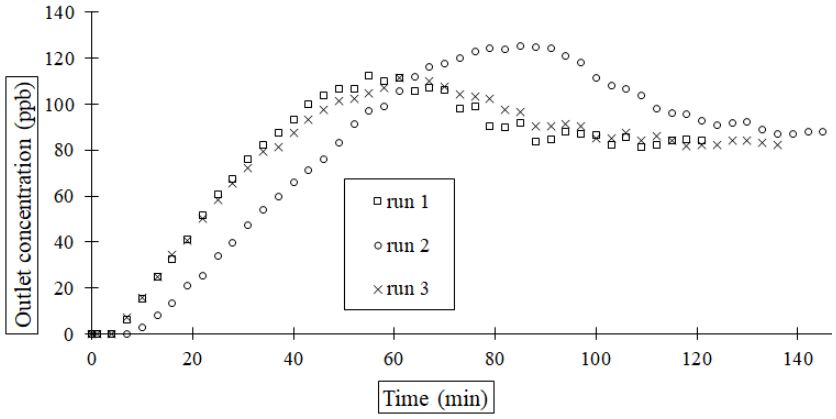

Figure 22: Adsorption profile at 25°C

II. Desorption

After getting the constant concentration at the column outlet, which was almost equal to the feed concentration, the flow of methyl iodide with air kept running through the column for almost 24 hours and then methyl iodide flow has been stopped. Air was then passed through the column until there was 0 ppb at the column outlet. It has been observed that the outlet concentration did not start from the constant concentration that has been observed at the time of adsorption. The average amount desorbed was 1.70 µg/g. The total time required for the desorption run was almost an hour.

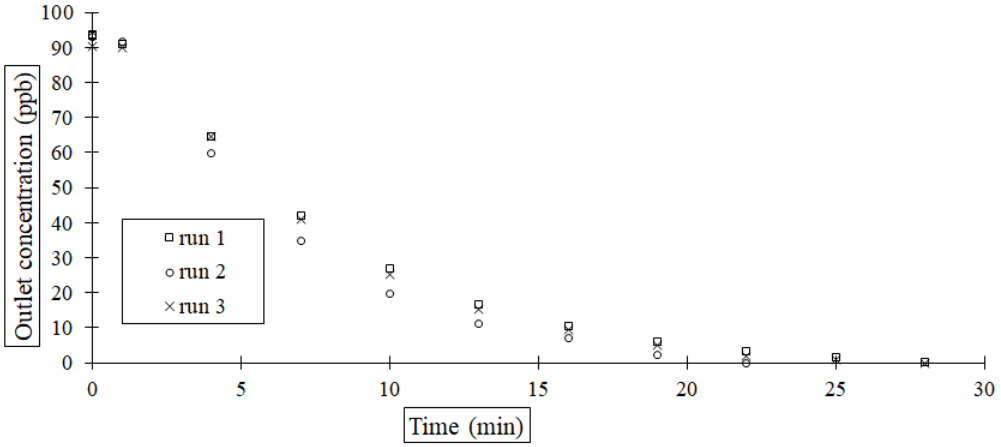

Figure 23: Desorption profile at 25°C

III. Comparative study of cycles

Three adsorption-desorption cycles were conducted to see the behavior of sodium mordenite. The amount desorbed in each run is similar and so is the adsorbed amount except run 2 as shown in table 5 and figure 23. The y-error bars indicate the deviation of amounts in each run as shown in figures 22 and 23. The trend of all three cycles was plotted as shown in figure 24. The combined adsorption and desorption runs are shown in figure 25.

Table 5: Cumulative amount adsorbed (µg/g) and desorbed (µg/g) per cycle at 25°C

Run	**The cumulative amount adsorbed and desorbed (µg/g)**	
	Desorption	**Adsorption**
Run 1	1.82	7.0
Run 2	1.55	10.18
Run 3	1.75	7.35

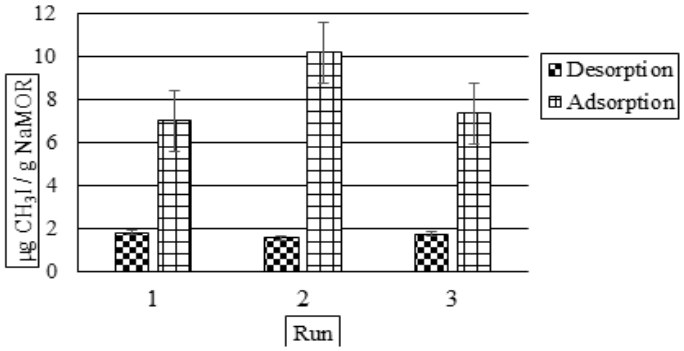

Figure 24: A plot for amount adsorbed and desorbed per run at 25°C

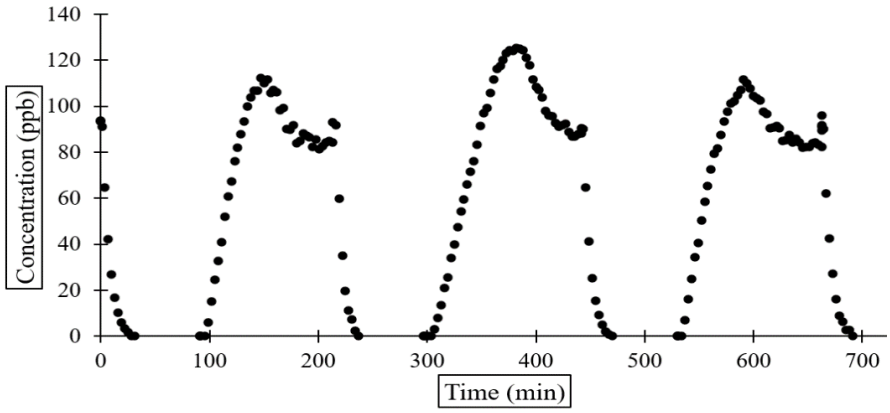

Figure 25: Adsorption – desorption cycles at 25°C

C] Adsorption – desorption cycles at 70°C

After the cycles at 25 °C were over, the temperature was then increased to 70°C. After 2 days the cycles have been performed and the behavior is as shown in figures 26 and 27. Until then, the adsorbent was subjected to saturation.

I. Adsorption

The average amount adsorbed was 14.39 µg/g. The time required for the adsorption was nearly 2.5 hours same as cycles at 25°C.

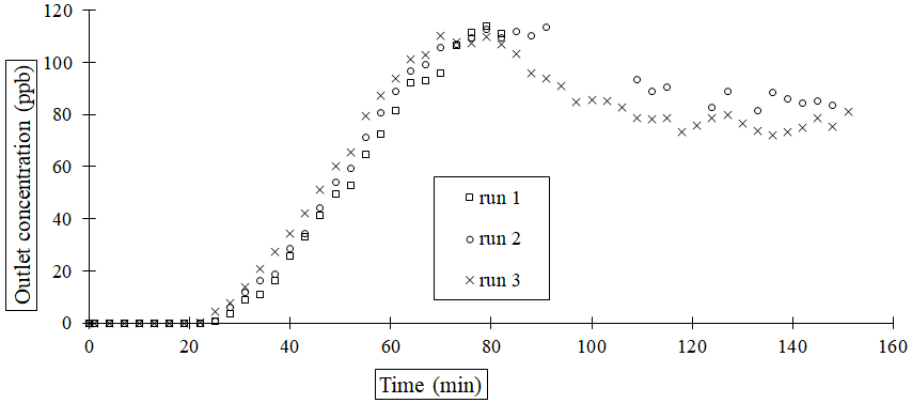

Figure 26: Adsorption profile at 70°C

II. Desorption

The average amount desorbed was 4.13 µg/g. The total time required for the desorption run was almost an hour.

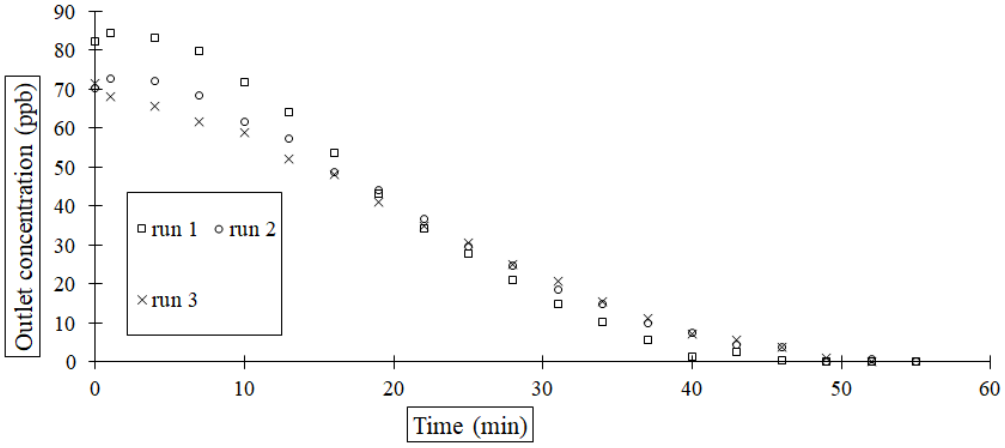

Figure 27: Desorption profile at 70°C

III. Comparative study of cycles

Like the cycles at 25°C, there is no change in the amount adsorbed per run and so is the amount desorbed as shown in table 6. Different cycles were plotted as shown in figure 28.

Table 6: Cumulative amount adsorbed (µg/g) and desorbed (µg/g) per cycle at 70°C

Run	The cumulative amount adsorbed and desorbed (µg/g)	
	Desorption	Adsorption
Run 1	4.29	15.04
Run 2	4.15	14.42
Run 3	3.97	13.72

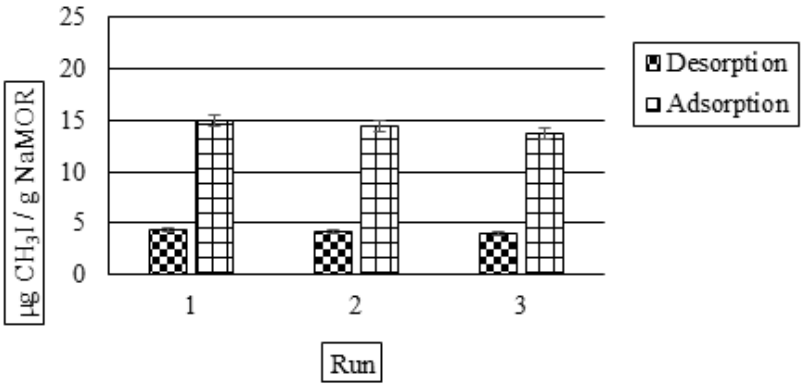

Figure 28: A plot for amount adsorbed and desorbed per run at 70°C

The combined adsorption-desorption cycles behavior is as shown in figure 29.

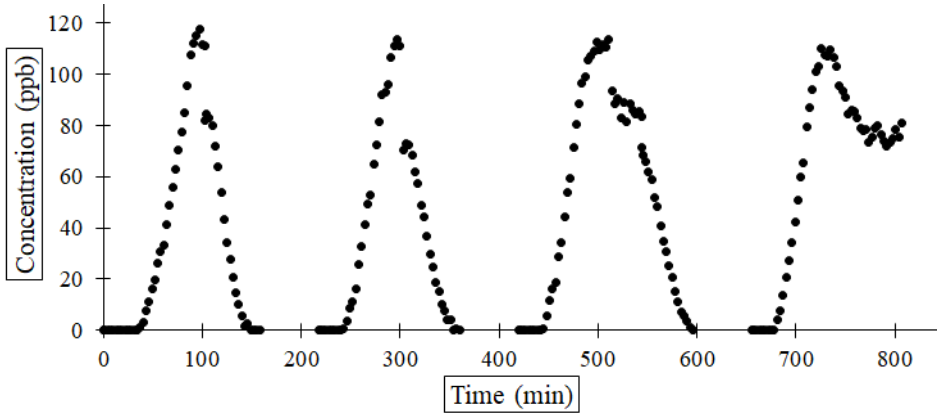

Figure 29: Adsorption – desorption cycles at 70°C

D] Adsorption – desorption cycles at 120°C

I. Adsorption

The average amount adsorbed is 11.82 µg/g and the time required for the adsorption was nearly 2.5 hours. All the performed adsorption cycles are as shown in figure 30.

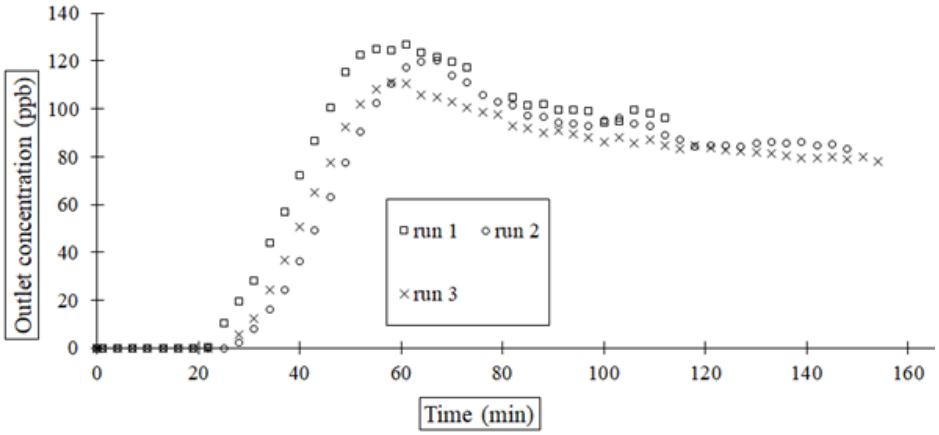

Figure 30: Adsorption profile at 120°C

II. Desorption

The average amount desorbed is 4.28 µg/g. The total time required for the desorption run was almost an hour. All the performed desorption cycles are as shown in figure 31.

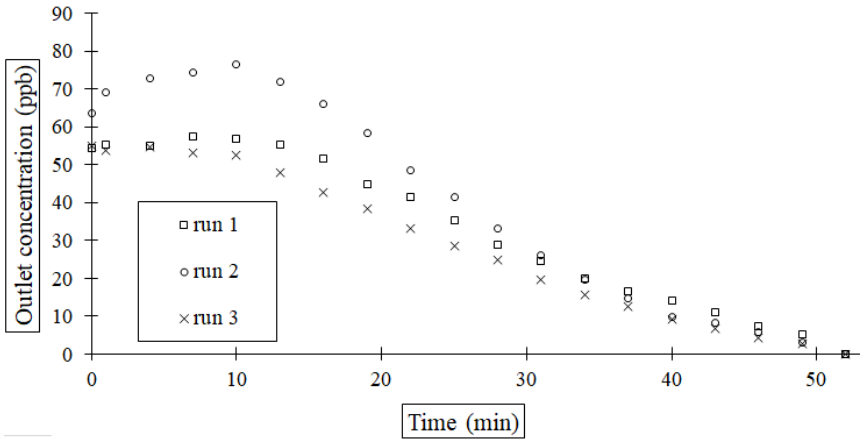

Figure 31: Desorption profile at 120°C

III. Comparative study of cycles

The amount adsorbed and desorbed did not vary for different cycles as shown in table 7 figure 32.

Table 7: Cumulative amount adsorbed (µg/g) and desorbed (µg/g) per cycle at 120°C

Run	**The cumulative amount adsorbed (µg/g)**	
	Desorption	**Adsorption**
Run 1	4.19	10.61
Run 2	5.05	12.87
Run 3	3.61	12

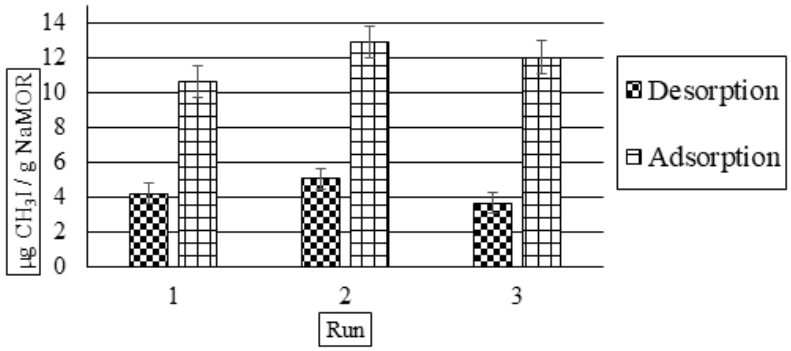

Figure 32: A plot for amount adsorbed and desorbed per run at 120 °C

All the adsorption-desorption cycles are as shown in figure 33.

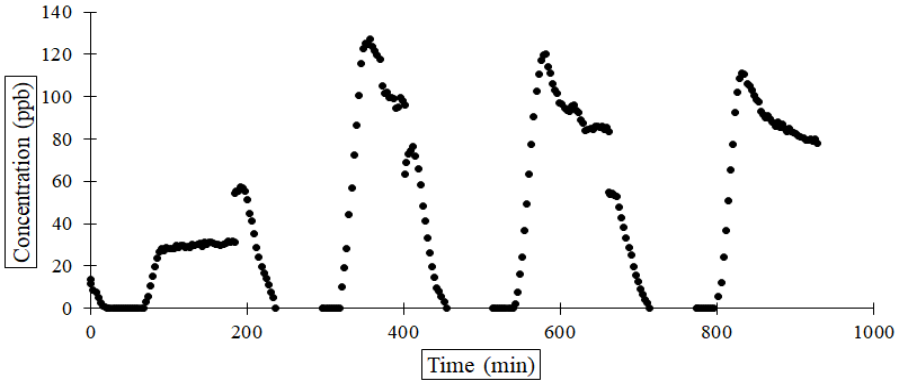

Figure 33: Adsorption – desorption cycles at 120°C

E] Adsorption – desorption cycles at 170°C

The results of the amount adsorbed and desorbed for each cycle are discussed as follows.

I. Adsorption

The average amount adsorbed is 12.33 µg/g and the time required for the adsorption was nearly 2.5 hours. All the adsorption cycles are as shown in figure 34.

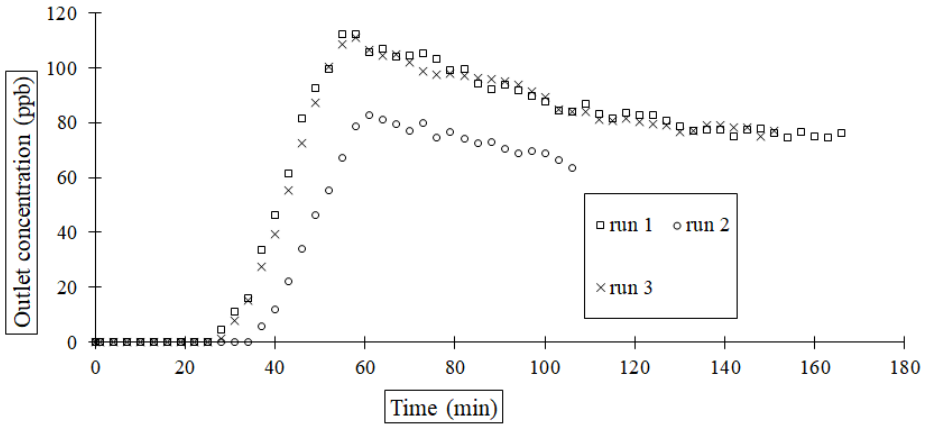

Figure 34: Adsorption profile at 170°C

II. Desorption

The average amount desorbed is 4.05 µg/g and the total time required for the desorption run was almost an hour. All the desorption cycles are as shown in figure 35.

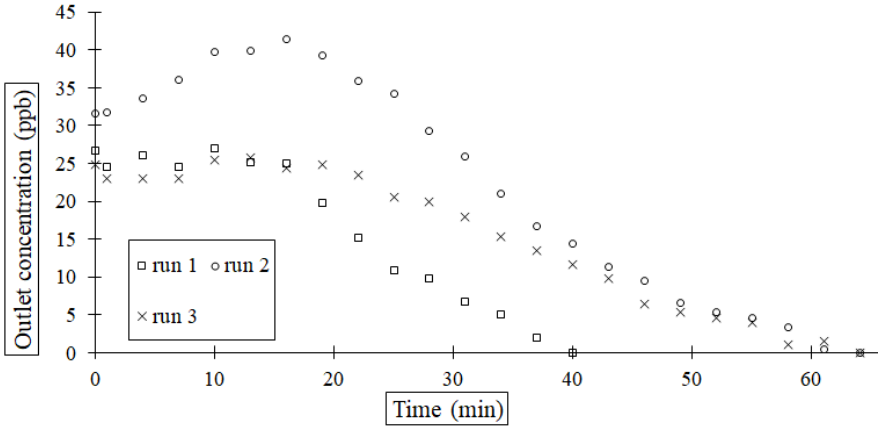

Figure 35: Desorption profile at 170°C

III. Comparative study of cycles

A set of two cycles state that there is no change in the amount adsorbed and desorbed as shown in table 8 and figure 36.

Table 8: Cumulative amount adsorbed (µg/g) and desorbed (µg/g) per cycle at 170°C

Run	**The cumulative amount adsorbed (µg/g)**	
	Desorption	**Adsorption**
Run 1	3.49	12.16
Run 2	2.36	12.51

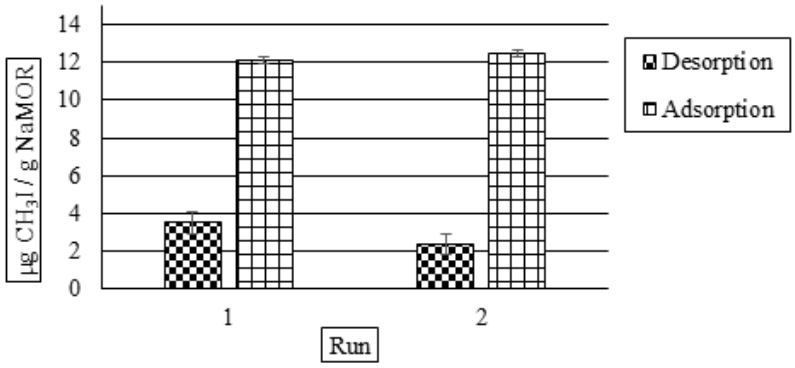

Figure 36: A plot for amount adsorbed and desorbed per run at 170°C

The adsorption cycles followed by desorption cycles are as shown in figure 37.

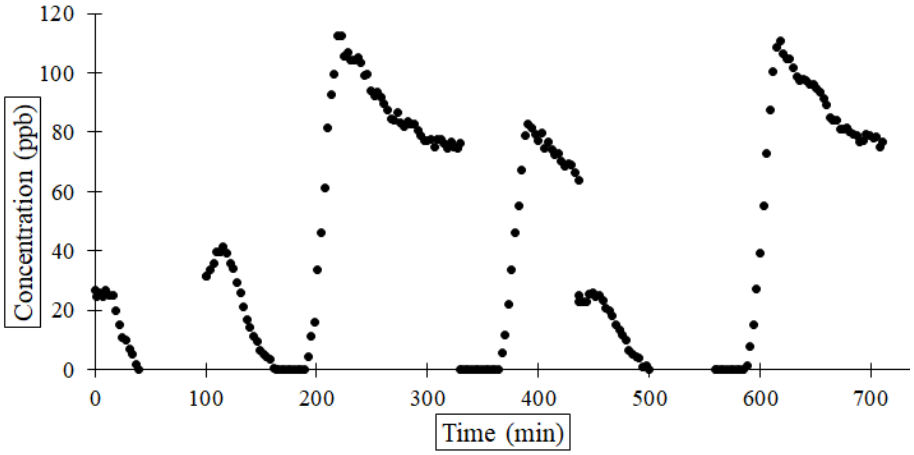

Figure 37: Adsorption – desorption cycles at 170°C

3.2.3.2 FEPE (Fluorinated ethylene propylene) column

A] Adsorption – desorption cycles at 25°C

The results from adsorption-desorption cycles at 25°C are discussed as follows:

I. Adsorption

The average amount adsorbed is 11.28 µg/g and the time required for the adsorption was nearly 2.6 hours. The adsorption cycles are as shown in figure 38.

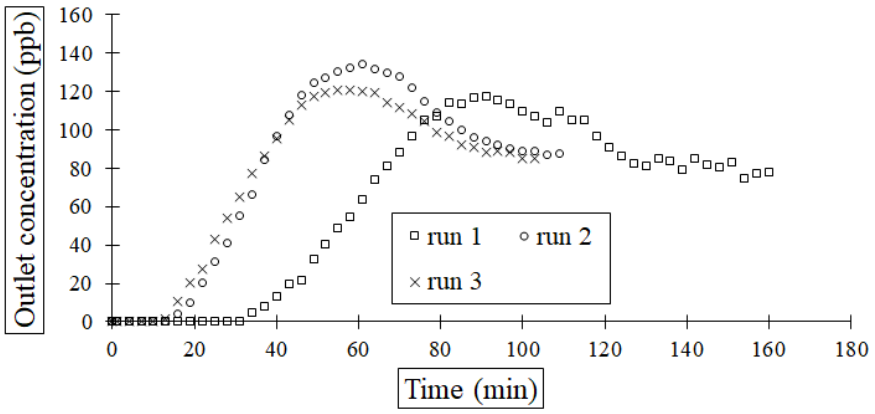

Figure 38: Adsorption profile at 25°C

II. Desorption

The average amount desorbed is 2.57 µg/g and the total time required for the desorption run was almost an hour. The desorption cycles are as shown in figure 39.

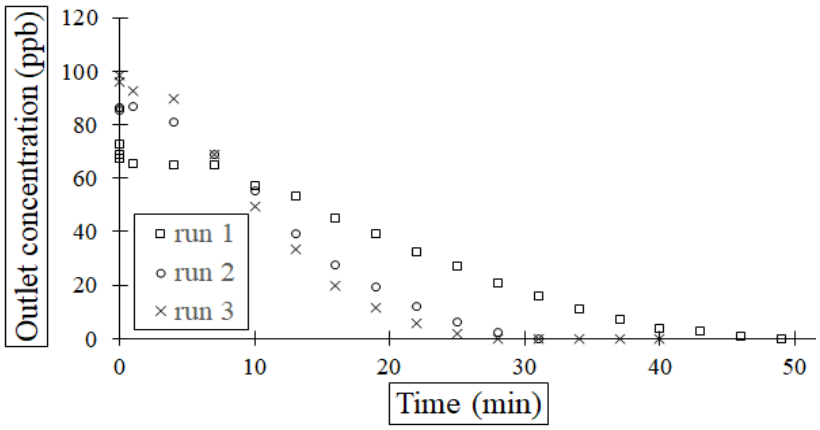

Figure 39: Desorption profile at 25°C

III. Comparative study of cycles

Different adsorption-desorption cycles at 25°C indicate that there is a physisorption of iodine species. But, it was found as unlike in the SS316 column, it doesn't possess the same amount adsorbed and desorbed for all the cycles as shown in table 9 and figure 40.

Table 9: Cumulative amount adsorbed (µg/g) and desorbed (µg/g) per cycle at 25°C

Run	**The cumulative amount adsorbed (µg/g)**	
	Desorption	**Adsorption**
Run 1	3.68	16.7
Run 2	1.42	8.88
Run 3	2.62	8.28

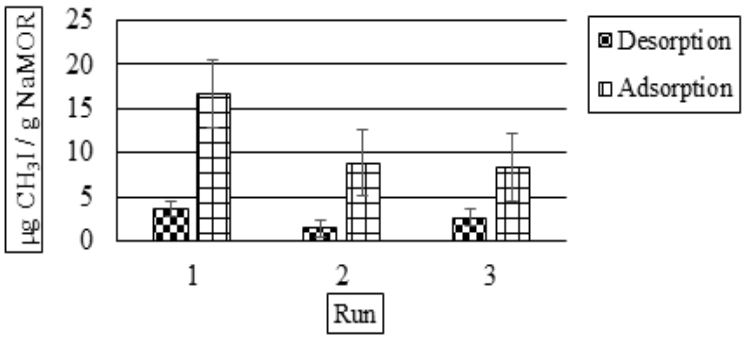

Figure 40: A plot for amount adsorbed and desorbed per run at 25°C

B] Adsorption – desorption cycles at 70°C

I. Adsorption

The average amount adsorbed is 9.0 µg/g and the time required for the adsorption was nearly 2 hours. The adsorption cycles are as shown in figure 41.

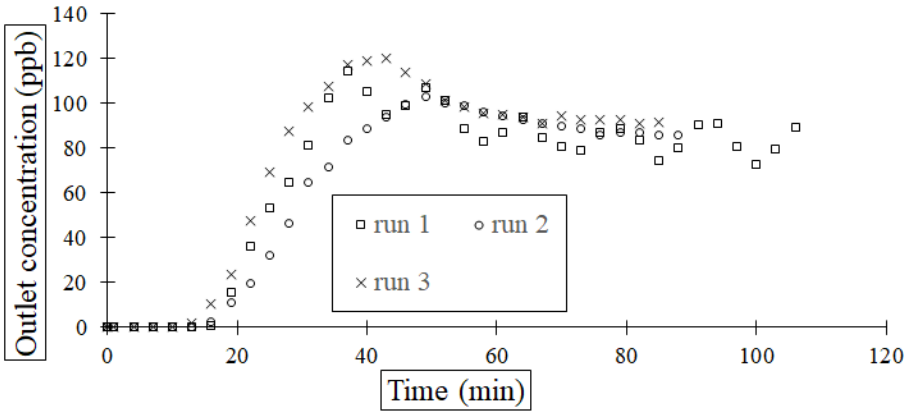

Figure 41: Adsorption profile at 70°C

II. Desorption

The average amount desorbed was 2.46 µg/g and the total time required for the desorption run was almost an hour. The desorption cycles are as shown in figure 42.

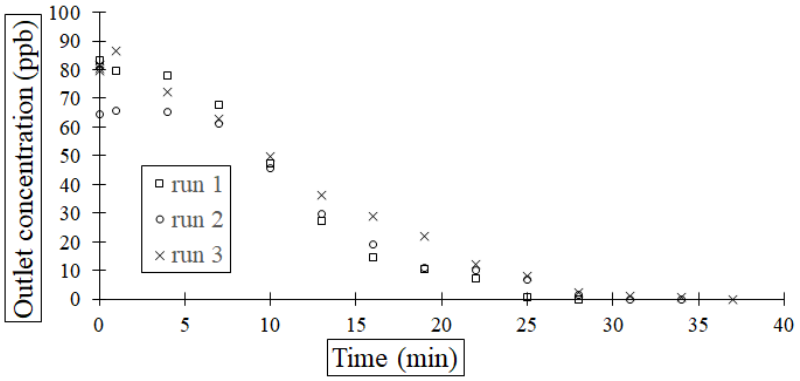

Figure 42: Desorption profile at 70°C

III. Comparative study of cycles

Unlike the cycles at 70°C, the amount adsorbed and desorbed has not varied as shown in table 10 and figure 43. But, the amount desorbed can be called as amount physisorbed remained almost the same.

Table 10: Cumulative amount adsorbed (µg/g) and desorbed (µg/g) per cycle at 70°C

Run	**The cumulative amount adsorbed (µg/g)**	
	Desorption	**Adsorption**
Run 1	2.23	7.56
Run 2	2.69	10.44

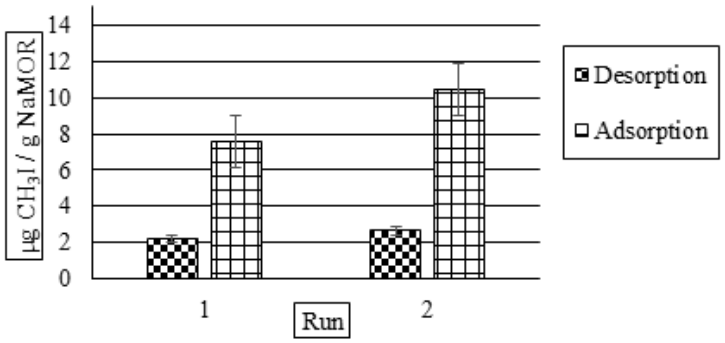

Figure 43: A plot for amount adsorbed and desorbed per run at 70°C

C] Adsorption – desorption cycles at 120°C

The temperature was increased to 120°C to see the effect of high temperature. When the adsorption cycle started at 120°C, the outlet concentration was found to be almost zero ppb. It could be

the possibility that FEPE transformed into the rubber at 119°C and that could be the possible reason behind the zero outlet concentration.

3.2.4 Conclusion

The comparative results at all the temperatures are as shown in figure 44.

3.2.4.1 Amount adsorbed and desorbed for SS column

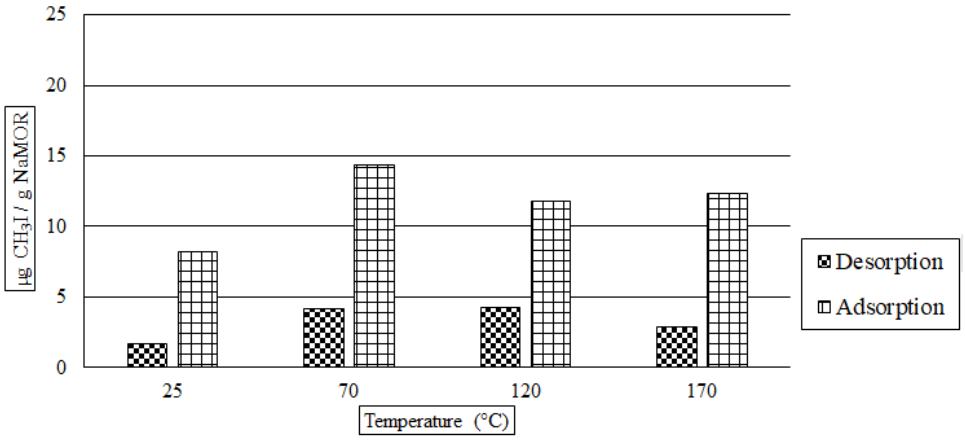

Figure 44: amount adsorbed and desorbed in a SS column

It was found that amount adsorbed and desorbed are not similar and they are affected by varying temperatures.

3.2.4.2 Amount adsorbed and desorbed for FEPE column: -

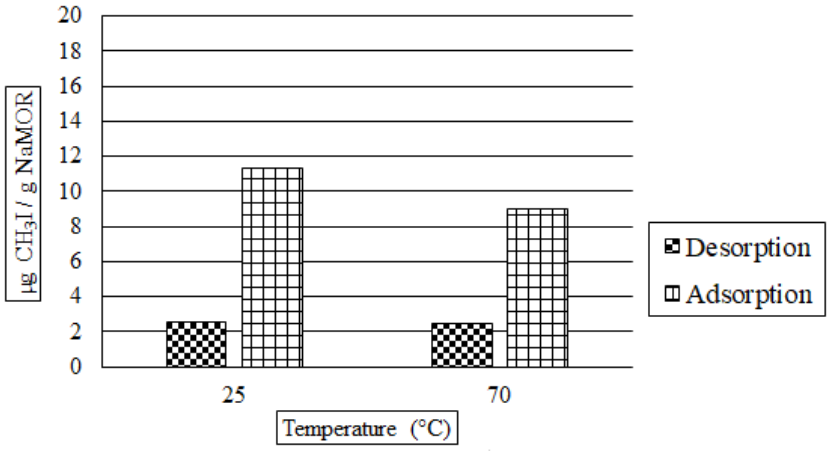

Figure 45: Amount adsorbed and desorbed in the FEPE column

Like SS316, the same result was found where FEPE is a material of construction. The amount adsorbed and desorbed was changed with the temperature as shown in figure 45.

3.2.4.3 Amount adsorbed and desorbed, SS versus FEPE

Table 11: SS316 vs FEPE comparison

Temperature (°C)	Desorption (µg/g)		Adsorption (µg/g)	
	SS 316	FEPE	SS 316	FEPE
25	1.7	2.57	8.17	11.28
70	4.13	2.46	14.39	9.0

The amount adsorbed and desorbed is changed with the material of construction. When SS 316 column was used, the amount adsorbed was more at high temperature. But, when FEPE was used, the amount adsorbed was found to be less. The amount desorbed values were found to be relatively constant with respect to temperature for FEPE. But there's a change found when the SS316 column was used.

3.3 Adsorbents analysis

3.3.1 Characterization of the adsorbents

Structural and compositional analysis has been done to find out the adsorbents characteristics which are discussed as follows.

3.3.2 BET surface area analysis

BET describes the physisorption of gas molecules on the solid surface of the adsorbent. BET surface area (m^2/g) gives an idea about the adsorption capacity of the sorbent. The equipment used for surface area analysis is the Micromeritics Flowsorb II 2300 surface area analyzer as shown in figure 46.

Figure 46: Flowsorb II 2300 [25]

The surface area for all the adsorbents was found as follows:

Table 12: Surface area distribution of adsorbents

Type of adsorbent	Surface area (m^2/g)
Sodium mordenite	341
Partially exchanged (3.8%) silver mordenite	321
Partially exchanged (63%) silver mordenite	271
Fully exchanged (100%) silver mordenite	216

It was seen that the surface area got decreased after the exchange with silver. The silver atoms are bigger and they might have occupied the pores and the surface area got decreased. BET surface area analysis states that sodium mordenite is more porous compare to silver exchanged mordenites and should possess good affinity towards iodine capture.

3.3.3 ICPMS technique (Inductively coupled plasma mass spectrometry technique)

ICPMS technique is generally used for the quantitative analysis of metals and non-metals. This mass spectrometry technique was used to determine silver content in the partially and fully exchanged silver mordenites. Ag present in the mordenites was extracted into the solution and the concentration of ions determined.

3.3.3.1 Sample extraction

The methods used to dissolve the silver mordenites to prepare the sample for the ICPMS analysis are discussed as follows:

A] EPA 3050B

The sample was crushed and weighed. 10 mL 1:1 diluted HNO_3 was added and mixed. It was covered with a watch glass and heated to 95 °C and refluxed for 10-15 minutes without boiling. The sample was allowed to cool. 5 ml of concentrated HNO_3 was added and refluxed for 30 minutes. The solution was then allowed to evaporate to approximately 5 mL volume without boiling at 95 °C for 2 h. After cooling, 2 mL water and 3 mL of 30% H_2O_2 were added. The solution was then heated until it effervesced and then it was cooled down. Adding 30% H_2O_2 in 1 mL aliquots was continued with warming until effervescence was minimal. 10 mL 30% H_2O_2 was added in total. The solution was heated until the volume was reduced to approximately 5 mL at 95 °C for 2 h. After cooling, the solution was diluted to 100 ml with water. The solution was centrifuged at 2000-3000 rpm for 10 min [26].

B] Ion-exchange

An attempt of the sample dissolution was made using conc. HNO_3. The sample was taken and then mixed with 200 ml water and 200 ml HNO_3. The solution was then refluxed for 2 hours at 90°C. 10 ml of the solution was taken and centrifuged for 10 minutes at the speed of 2000 rpm. This 10 ml

was diluted ten-fold by adding 90 ml DI water. The reflux time was increased to 6 hrs. for the second digestion, first ion-exchange and so is the amount of sample. For the second exchange, the remaining solids from the exchange 1 sample were separated with the help of a centrifuge. The undissolved solids sample was taken and the sample was prepared following the digestion procedure as discussed earlier.

The expected silver content and actual silver extraction results are different for all the implemented methods. None of the methods was able to extract the present silver in the sample. The results are shown in table 13 and 14 which is as follows:

Table 13: Silver extraction comparison of different methods for partially exchanged silver mordenite

Method			**Amount of AgMOR taken for sample (g)**	**Expected Ag (µg/L)**	**Ag by ICPMS (µg/L)**	**% discrepancy**
EPA 3050B			0.0023	3500	1700	51.42
Ion Exchange	**Digestion 1**		0.1044	4071.72	3300	18.95
	Digestion 2	**Exchange 1**	0.1052	4102.92	3600	12.25
		Exchange 2	0.1052	1855.71	20	98.92

Table 14: Silver extraction comparison of different methods for fully exchanged silver mordenite

Method			**Amount of AgMOR taken for sample (g)**	**Expected Ag (µg/L)**	**Ag by ICPMS (µg/L)**	**% discrepancy**
EPA 3050B			0.0028	6390	3100	51.48
Ion Exchange	**Digestion 1**		0.1021	5865.89	3900	33.51
	Digestion 2	**Exchange 1**	0.1054	6055.48	4200	30.64
		Exchange 2		1661.44	12	99.27

Comparing the percent discrepancy for the two processes mentioned, sample dissolution through ion exchange gave good results, but still, it served as a semiquantitative analysis technique as it was unable to dissolve all the present silver, which is the reason for the discrepancy in actual and expected silver content.

3.3.4 Scanning electron microscopy (SEM) imaging

In the characterization of the adsorbent, SEM plays an important role. Scanning electron microscopy gives information about the structure of the surface. SEM imaging is done to compare different adsorbents such as sodium mordenite, partially exchanged silver mordenite, and fully exchanged silver mordenite using SEM 35VP instrument. The surface of the adsorbents was viewed at 1000X magnification with 10 µm of resolution.

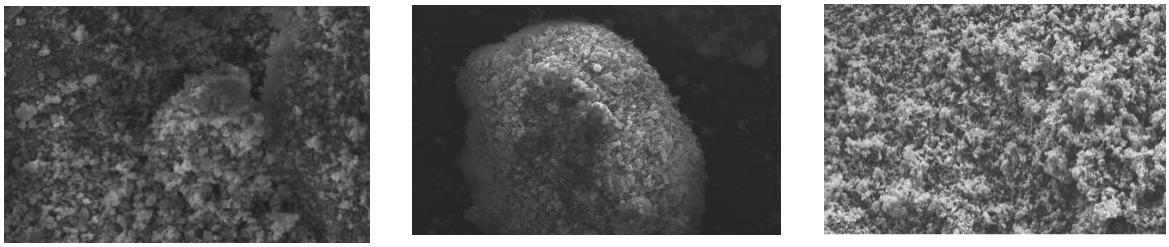

Sodium mordenite | Partially exchanged AgMOR | Fully exchanged AgMOR

(a) Before the adsorption experiment

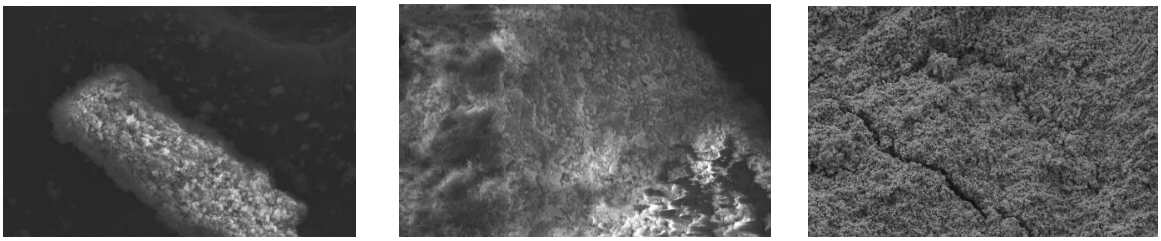

Sodium mordenite | Partially exchanged AgMOR | Fully exchanged AgMOR

(b) After the adsorption experiment

Figure 47: SEM imaging of the adsorbents

It was seen that the adsorbent was porous before the adsorption experiment and it was no longer porous as it was before the adsorption experiment as shown in figure 47. There is no morphological change throughout the synthesis process in both partially and fully exchanged silver mordenite. Although, there is a change in surface area.

3.3.5 Energy dispersive x-ray spectroscopy (EDS)

Energy dispersive x-ray spectroscopy was done to obtain the elemental composition in different adsorbents before and after their activation as shown in table 15.

Table 15: Compositional detection of silver before and after activation of the sorbents

Partially exchanged AgMOR			**Fully exchanged AgMOR**		
Ag expected(g)	Ag detected before activation (g)	Ag detected after activation (g)	Ag expected(g)	Ag detected before activation (g)	Ag detected after activation (g)
2.6676	2.5597	0.8658	4.212	2.942	3.8258

This analysis was done at different points on the surface of the sample. Energy dispersive x-ray analysis has been performed to study the behavior of iodine loading according to the type of mordenite and weight percent of silver. It was found that there is a difference in the iodine loading with the variation in silver content which is discussed as shown in figure 48.

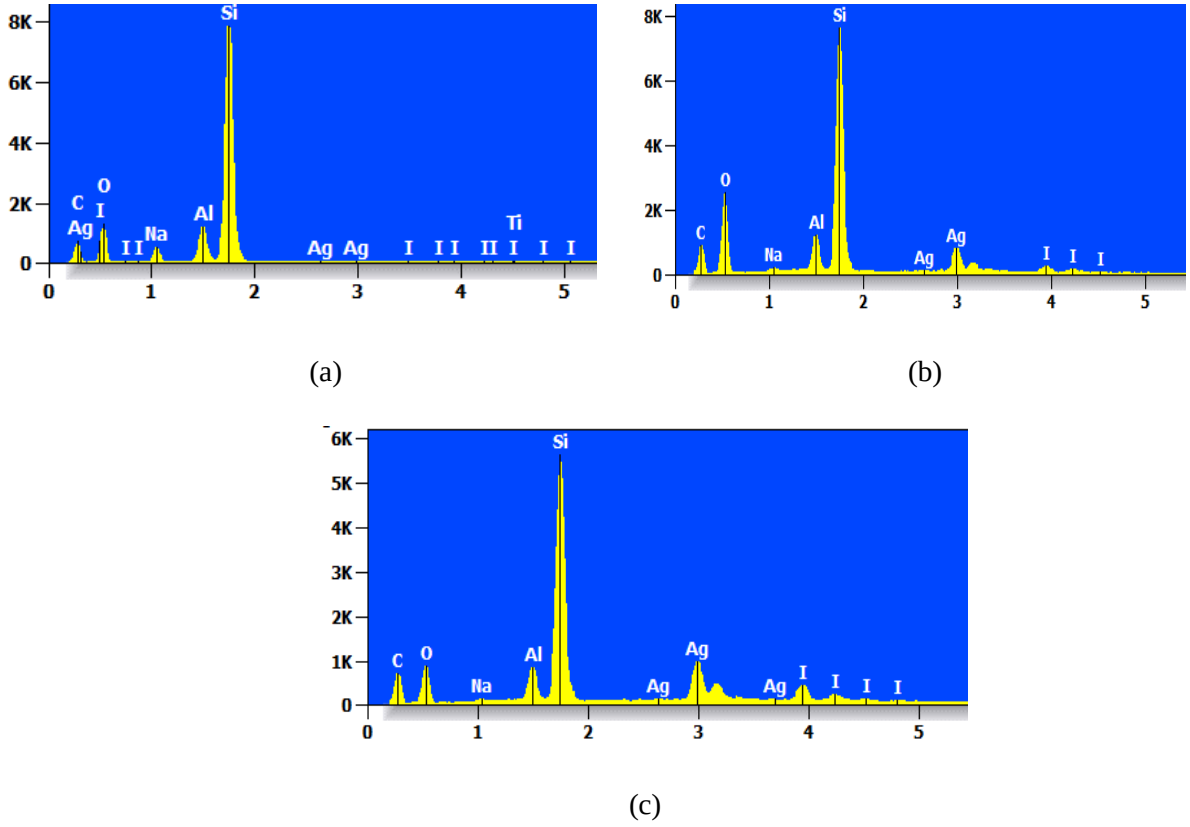

(a) Sodium mordenite (b) Partially exchanged silver mordenite (c) Fully exchanged silver mordenite

Figure 48: Iodine loading variation

Table 16: Analysis of iodine loading

Name of the adsorbent	The weight percent of silver	The weight percent of iodine
Sodium mordenite	0	0.26
Partially exchanged silver mordenite	15	2.34
Fully exchanged silver mordenite	23	10.86

The analysis results support the fact that an increase in silver content helps to increase iodine loading as shown in table 16.

3.3.6 X-ray diffraction analysis (XRD)

XRD analysis was done to find out the crystalline nature of the adsorbents. It was done to see the nature of the adsorbent before and after the adsorption experiment. It was found that there is no change in the crystalline nature of all three adsorbents before and after the adsorption experiment.

3.3.7 Residence time and final concentration after adsorption trend

When the residence time increases, the column outlet concentration decreases as shown in figure 49. The outlet concentration reached zero with more residence time. The silver content, as well as appropriate residence time, allows better capture of iodine species.

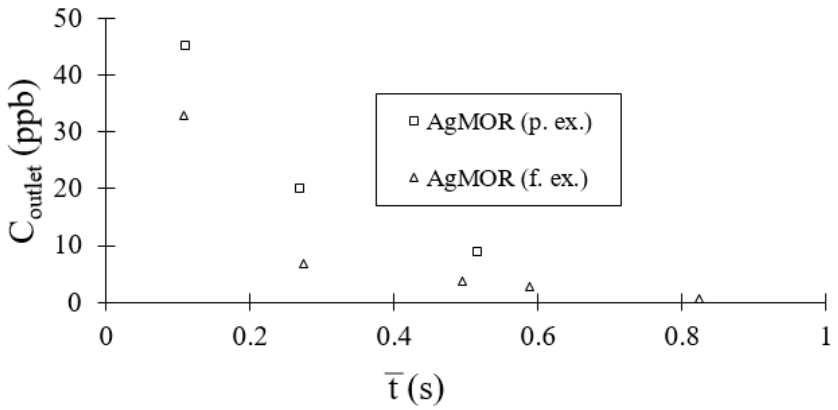

Figure 49: Residence time and column outlet concentration relation

3.3.8 Draeger tube analysis

Considering no breakthrough occurrence, it was decided to verify the decomposition of methyl iodide. The Draeger tube analysis was performed to determine the decomposition assumption which is described below:

3.3.8.1 Sodium mordenite

It was reported that sodium mordenite favors the physical adsorption of iodine species. The reaction mechanism can be as follows:

$$CH_3I\ (g) + Na \rightarrow NaI + CH_3^{\bullet}$$

$$NaI + CH_3^{\bullet} + Na + CH_3I\ (g) \rightarrow 2NaI + C_2H_6\ (g) \uparrow$$

The Draeger tube test was also performed to check if there is the decomposition of CH_3I to I_2.

Figure 50: Draeger tube analysis for sodium mordenite

The feed gas was passed through the column at the flow rate of 0.25 L/min for one hour. A color change was observed in the Drager tube from yellow to pink up to the marking of 0.2 ppm for 500 ml of the gas as shown in figure 50. A total of 15 L of gas was passed and 6.67 ppb of I_2 was found. The feed gas was also checked to see if there is decomposition happening or not. I_2 was not found in the feed to the column. But it did confirm the decomposition reaction.

3.3.8.2 Partially exchanged silver mordenite

The Draeger tube test was performed for partially exchanged silver mordenite as well to determine the decomposition of methyl iodide. The Draeger tube results report no color change as shown in figure 51 and that indicates there is no decomposition of methyl iodide or it was not detectable using this technique.

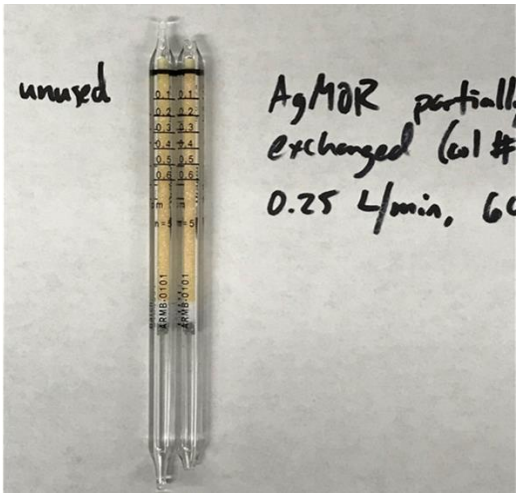

Figure 51: Draeger tube analysis for partially exchanged silver mordenite

3.3.8.3 Fully exchanged silver mordenite

The Draeger tube test was also performed for fully exchanged silver mordenite but like partially exchanged silver mordenite, there was no color change occurred as shown in figure 52 and which implies there is no decomposition of methyl iodide.

Figure 52: Draeger tube analysis for fully exchanged silver mordenite

I_2 was not detected for all the three adsorbents and sorbent exhaustion was never achieved as well. The possible scenario about the reaction kinetics and mass transfer analysis is discussed in chapter 4.

Chapter 4: Reaction kinetics and mass transfer dynamics

Various investigations are done to hypothesize reaction kinetics and mass transfer dynamics which is explained in this chapter.

4.1 Reaction mechanism

It was found that the final concentrations after reaction with adsorbents were never matched to the feed concentration. It could be a possibility that none of the adsorbents got exhausted as it was still adsorbing incoming iodine species. It can be hypothesized; the adsorption column is no longer behaving as a pure adsorption column, but as a reactor effecting some reaction.

It was also found that the feed concentration and final concentration after adsorption were not equal but constant over time. It was then hypothesized that there can be a decomposition of methyl iodide as it was not accounting for the difference between initial and final concentration. The constant inlet and outlet concentrations lead to the possibility that the reaction attained a steady state. That could be the possible reason for not getting the breakthrough.

4.1.1 Fully exchanged silver mordenite

Flow rates were varied from 0.33 L/min to 1.33 L/min and the concentration changes were monitored. The inlet concentration was nearly 140 ppb and kept constant. The outlet concentration is varied with the changing flow rates. As the flow rate changed, the column outlet concentration approached 70 ppb. It was observed that it was not that much closer to the inlet concentration as it was seen for the partially exchanged silver mordenite as shown in figure 53.

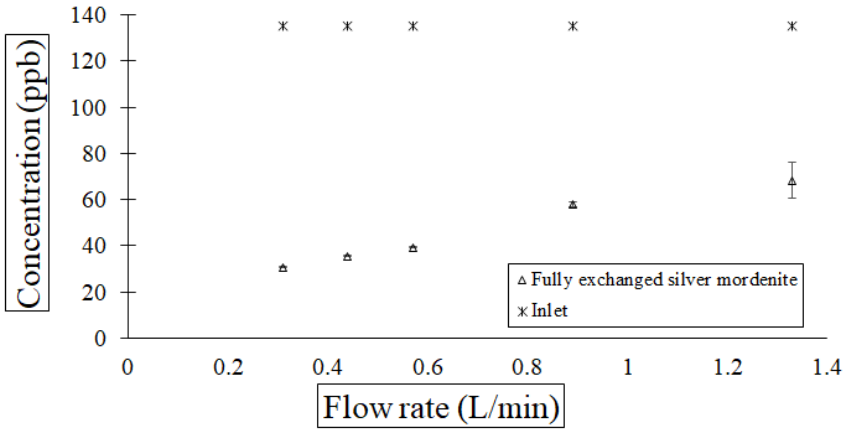

Figure 53: Concentration vs flow rate

To find the reaction order for the fully exchanged silver mordenite, the residence time is calculated for all the tried flow rates as shown in table 17 and the plots are made for zero, first and second order.

Table 17: Flow rates and conversions

Flow rate (L/min)	**$\bar{t}$ (s)**	**$[A]_0$ (ppb)**	**[A] (ppb)**	**X_A**
0.31	0.39	135	30.76	0.77
0.44	0.28	135	35.49	0.74
0.57	0.21	135	39.31	0.71
0.89	0.14	135	57.83	0.57
1.33	0.092	135	68.3	0.49

4.1.1.1 Zero-order

By using the integral method, the plot is made.

For the zero order,

$$[A] = [A]_0 + k.\,\bar{t}$$

Where,

[A] = final concentration in ppb

$[A]_0$ = Initial concentration in ppb

$\bar{t}$ = residence time (s)

k = reaction rate constant

In terms of conversion, it can be written as,

$$X_A = \frac{(-k)\bar{t}}{[A]0}$$

Comparing this equation to the equation of a straight line, X_A vs $\bar{t}$ is plotted.

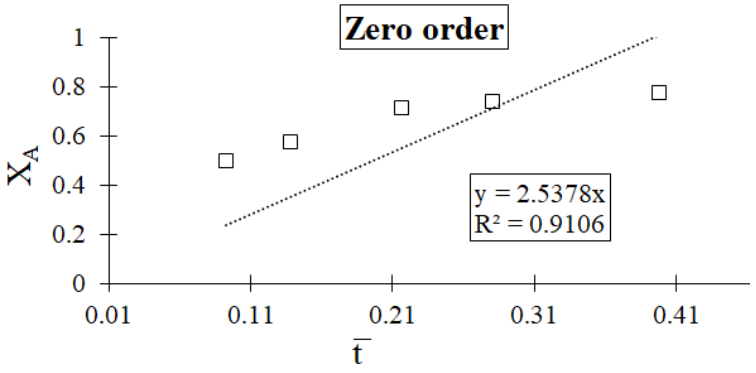

Figure 54: Zero-order curve fit

The curve fit for the zero-order is not perfect as the points are scattered and not lying on a straight line as shown in figure 54 and thus rule out the possibility of zero order.

4.1.1.2 First order

By using the differential method, the plot is made as shown in figure 55.

For the first order,

$$\ln [A] = -k\,\bar{t} + \ln [A]_0$$

Where,

[A] = final concentration in ppb

$[A]_0$ = Initial concentration in ppb

$\bar{t}$ = residence time (s)

k = reaction rate constant

In terms of conversion, it can be written as,

$$\ln \left[\frac{1}{1-XA}\right] = k\,\bar{t}$$

Comparing this equation to the equation of a straight line, $\ln \left[\frac{1}{1-XA}\right]$ vs $\bar{t}$ is plotted.

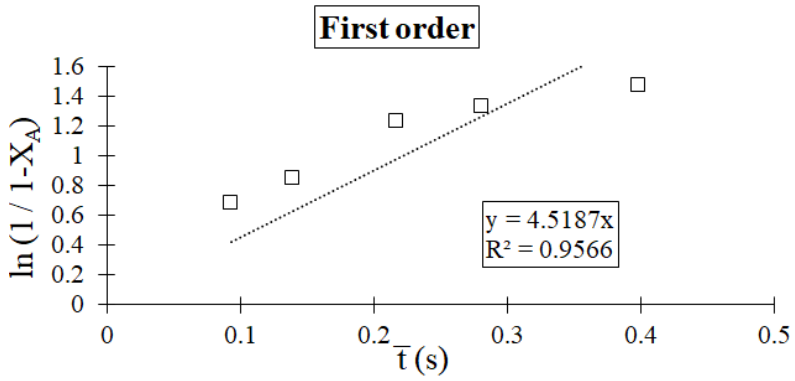

Figure 55: First order curve fit

The curve fit for the first order is good to compare to the zero-order plot.

From the plot, k = 4.5187 s^{-1}

4.1.1.3 Second-order

By using the differential method, the plot is made as shown in figure 56.

For the second-order,

$$\frac{1}{[A]} = -k\,\bar{t} + \frac{1}{[A]0}$$

Where,

[A] = final concentration in ppb

$[A]_0$ = Initial concentration in ppb

$\bar{t}$ = residence time (s)

k = reaction rate constant

In terms of conversion, it can be written as,

$$\frac{XA}{1-XA} = k\,[A]_0\,\bar{t}$$

Comparing this equation to the equation of a straight line, $\frac{XA}{1-XA}$ vs $\bar{t}$ is plotted.

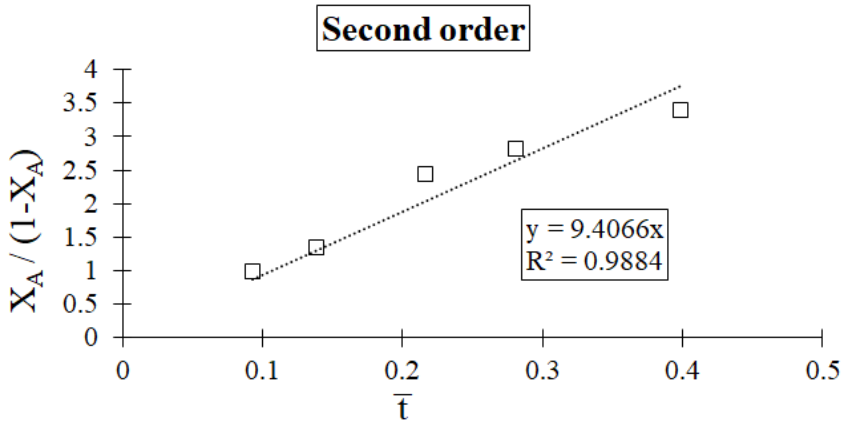

Figure 56: Second order curve fit

$$k\,[A]_0 = 9.4066$$

$$\therefore k = \frac{9.4066}{135} = 0.0696\ ppb^{-1}.s^{-1}$$

A] Possible reactions

$$CH_3I\ (g) + Ag^{\circ} \rightarrow AgI + CH_3^{\bullet}$$

$$AgI + CH_3^{\bullet} + Ag^{\circ} + CH_3I\ (g) \rightarrow 2AgI + C_2H_6\ (g) \uparrow$$

The rate expression can be written as:

$$(-r_A) = 0.0696\,[CH_3I]^2\ ppb/s$$

4.1.2 Partially exchanged silver mordenite

It was then decided to see the adsorption behavior at different flow rates and find the rate-controlling mechanism. Flow rates were varied from 0.33 L/min to 1.33 L/min and the concentration changes were monitored. The constant temperature of 170°C was maintained throughout all the variations of flow rates. The column was operated till the constant outlet concentration. The inlet concentration was around 140 ppb and kept constant. The column responds with different outlet concentrations with the changing flow rates. As the flow rate changed, the column outlet concentration approached the inlet concentration as shown in figure 57.

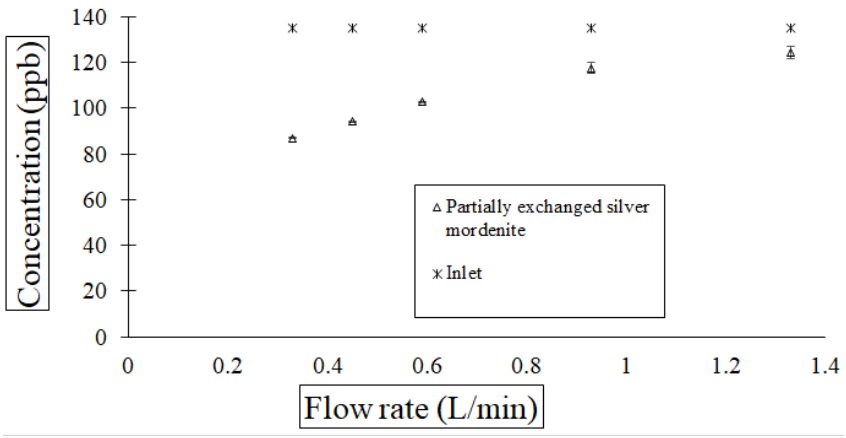

Figure 57: Concentration versus flow rate

The reaction mechanism for partially exchanged silver mordenite can be written as,

$$Na - Ag° (s) + CH_3I (g) \rightarrow Na\text{-}AgI (s) + CH_3^{\cdot}$$

$$Na\text{-}AgI (s) + CH_3^{\cdot} + Na - Ag° (s) + CH_3I (g) \rightarrow 2AgI (s) + 2NaI + C_2H_6 (g) \uparrow$$

Various curve fittings were done to find out the reaction order as shown in figure 58.

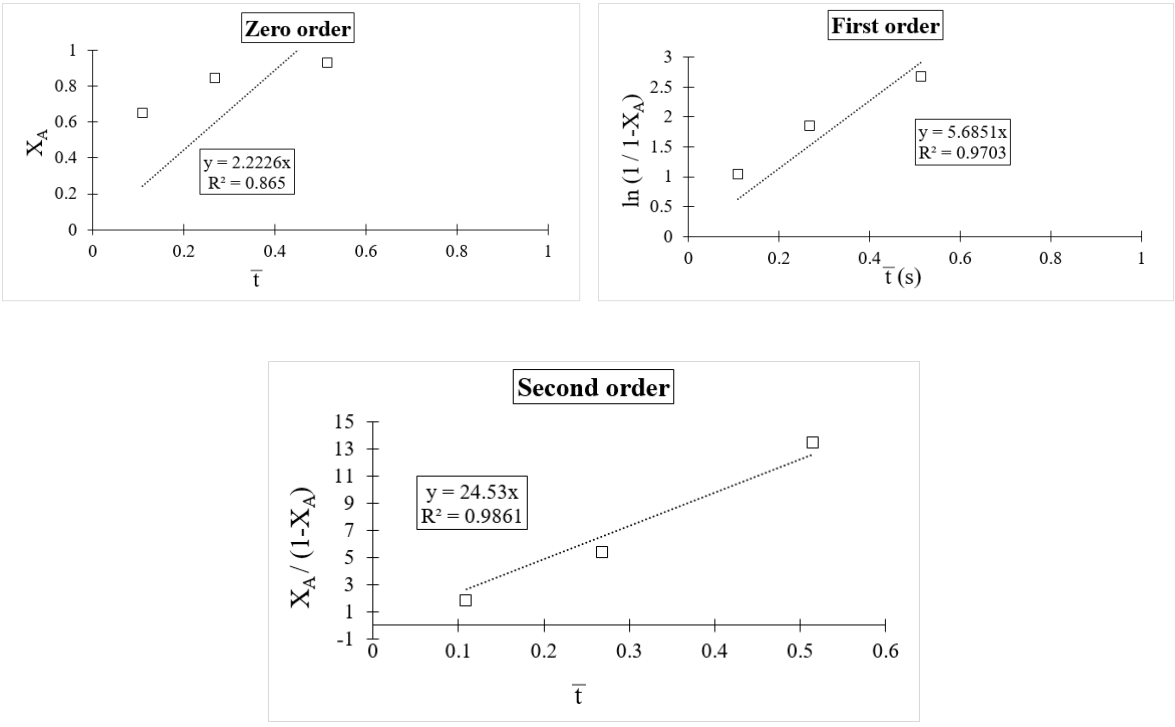

Figure 58: Curve fittings for zero, first, and second-order

For the fully exchanged silver mordenite, second-order kinetics fits more accurately. But, for the partially exchanged silver mordenite, neither first nor second-order curves have given robust confirmation about the order. Although, the regression value for the second-order justifies the second-

order well compare to the first order. Therefore, second-order kinetics of fully exchanged silver mordenite were tried to fit for the partially exchanged silver mordenite as follows:

Rate constant (k) α Ag present

$$\therefore k_{column\ 2} = 0.63.\ k_{column\ 3}$$

$$\therefore k_{column\ 2} = 0.63 \times 0.0696 = 0.044\ (ppb^{-1}.s^{-1})$$

$$(-r_A) = 0.044\ [CH_3I]^2\ ppb/s$$

In terms of conversion, a second-order equation can be written as,

$$\frac{X_A}{1-X_A} = k\ [A]_0\ \bar{t}$$

$\frac{X_A}{1-X_A}$ was calculated for all the flow rates and thereby, X_A was calculated as well for all the flow rates to find the expected column outlet concentration.

Table 18: Observed and expected column outlet concentrations

Flow rate (L/min)	**$\bar{t}$ (s)**	**$[A]_0$ (ppb)**	**$[A]_{obs.}$ (ppb)**	**$X_{A,\ obs.}$**	**Expected X_A (n=2)**	**[A] (ppb) (n=2)**	**Expected X_A (n=1)**	**[A] (ppb) (n=1)**
0.33	0.37	135	87.06	0.35	0.68	41.96	0.65	46.47
0.45	0.27	135	94.17	0.30	0.61	60.26	0.44	74.35
0.59	0.20	135	102.71	0.23	0.55	51.40	0.54	61.76
0.93	0.13	135	117.65	0.12	0.44	75.55	0.31	92.47
1.33	0.09	135	124.28	0.07	0.35	87.08	0.23	103.61

The observed column outlet concentration did not match exactly with the expected outlet concentration for the first as well as second-order as shown in table 18.

4.2 Mass transfer dynamics

To find out the rate-controlling mechanism, the external mass transfer coefficient, k_g, is also calculated which was verified with the second Damkohler number (Da_{II}). The external mass transfer coefficient was calculated for partially and fully exchanged silver mordenite to predict the rate-controlling mechanism which is discussed as follows.

Following is the step by step used for the mass transfer coefficient calculations of fully exchanged silver mordenite.

4.2.1 Flow rate through the column, Qair (m^3/s)

$$Q_{air}\ (m^3/s) = Q_{air}\ (l/min) \times \frac{60}{1000}$$

4.2.2 Velocity through the column, vair (m/s)

$$v_{air}\ (m/s) = \frac{Qair}{Area\ of\ the\ column}$$

Known quantities:

d_{column} = 0.01016 m, r_{column} = 0.00508 m

h_{column} = 0.3048 m

$$\therefore v_{air}\ (m/s) = \frac{Qair}{\pi \times r \times r \times h}$$

4.2.3 Reynolds number (Re)

Known:

T = 170°C = 443 K

P = 101.325 kPa (1 bar)

ρ_{air} (kg / m³) = 0.7859 at 443 K and 101.325 kPa

μ_{air} (kg/m.s) = 0.00002485 at 443 K and 101.325 kPa

d_{pellet} (m) = 0.0011

For the Reynolds number calculation, most of the flow contains air. Hence, the physical properties of air are used.

$$Re = \frac{\rho_{air} \times v_{air} \times d(pellet)}{\mu_{air}}$$

4.2.4 D_v (diffusivity for gases)

$$D_v = \frac{1.013 \times 10^{-7} T^{1.75} \left(\frac{1}{M_a} + \frac{1}{M_b}\right)^{1/2}}{P\left[\left(\sum_a v_i\right)^{1/3} + \left(\sum_b v_i\right)^{1/3}\right]^2}$$

Where,

D_v = Diffusivity, m²/s

T = temperature in 'K'

M_a and M_b = molecular masses of component a and b (here, a is air and b is CH_3I)

P = total pressure in bar

Σv_i = dimensionless diffusion volume coefficient

4.2.5 Schmidt number (Sc)

Schmidt number is calculated using the formula mentioned below:

$$Sc = \frac{\mu_{air}}{\rho_{air} \times D_v}$$

4.2.6 Sherwood number (Sh)

For mass transfer correlation, Sherwood number is defined as follows:

$$Sh = 2 + 0.6\ Re^{0.5}\ Sc^{0.33},\ 0 \leq Re < 200,\ 0 \leq Sc < 250$$

4.2.7 Mass transfer coefficient, k_g

Mass transfer coefficient, k_g (m/s) can be calculated using the Sherwood number.

$$kg = \frac{Sh \times Dv}{d\ (pellet)}$$

4.2.8 k_g. a (s^{-1})

To compare the mass transfer coefficient with the reaction rate constant, a gas side mass transfer coefficient is calculated.

The specific area (m^2/m^3) is calculated to get k_g. a

$$k_g.a\ (s^{-1}) = k_g.a$$

A specific area, a, can be calculated as,

$$a = \frac{4}{d\ (pellet)}$$

Five different flow rates were tested and gas side mass transfer coefficients were also calculated for all flow rates as shown in table 19.

Table 19: Gas side mass transfer coefficients

Q_{air} (l/min)	**v_{air} (m/s)**	**Re**	**Sh**	**k_g (m/s)**	**k_g.a (1/s)**
0.33	0.0678	2.359	3.054	0.058	213.06
0.45	0.0924	3.2169	3.2314	0.062	225.40
0.59	0.1212	4.217	3.410	0.0654	237.86
0.93	0.1911	6.6483	3.7703	0.0723	262.99
1.33	0.2733	9.5078	4.1171	0.0789	287.17

4.3 Rate controlling mechanism

The second Damköhler for the interphase mass transfer was then determined to find the dominant mechanism. The rate constant for the second-order and external mass transfer coefficient were found and Da_{II} was calculated for partially and fully exchanged silver mordenite which is described as follows:

Second Damköhler number is defined as,

$$Da_{II} = \frac{\text{reaction rate}}{\text{diffusive mass}-\text{transfer rate}} = k.[A]_0^{\,n-1} / k_g.a$$

Second Damköhler number was determined at different flow rates for partially and fully exchanged silver mordenite as shown in table 20.

Table 20: Second Damköhler number

Flow rate (L/min)	**Da_{II} (Partially exchanged silver mordenite)**	**Da_{II} (Fully exchanged silver mordenite)**	**Peclet number (Pe)**
0.33	0.027	0.044	32.65
0.45	0.026	0.039	44.52
0.59	0.024	0.042	58.37
0.93	0.022	0.035	92.02
1.33	0.021	0.032	131.60

Second Damköhler number values imply that mass transfer is faster and the chemical reaction rate is slow and rate-controlling.

The peclet number (Pe) was also determined to study the extent of mixing as shown in table 20 and it was found as the system behavior is near plug flow conditions which indicate efficient adsorption.

It can be stated that the adsorption columns which were packed with adsorbents can be called a packed bed reactor in which the adsorbent is a catalyst. The findings are summarized and the possible future work in this realm is discussed in chapter 5.

Chapter 5: Conclusions and Future Work

The adsorption studies were conducted for methyl iodide capture using mordenites and the effect of the various parameter was studied.

5.1 Conclusions

Effective capture of the iodine species depends on the type of adsorbent and the type of adsorption mechanism. EDS and XRD analysis support the assumption that silver present in the adsorbent is the reason for the iodine species capture. Among all the three adsorbents, fully exchanged silver mordenite has more silver moles to adsorb iodine. The breakthrough results help this point as well. It was also found as when adsorbent was packed in the SS column, it adsorbs more in less time compared to the glass column. Adsorption – desorption cycles when performed at different temperatures in different materials of construction columns for sodium mordenite, it was found that the amount adsorbed or desorbed when SS column is similar to that in FEPE column.

The silver utilization for partially exchanged silver mordenite (15 wt.% Ag) and fully exchanged silver mordenite (23 wt. % Ag) was found as 43 % and 48% respectively. The adsorbents have succeeded in the capture of iodine species but none of the adsorbents has ever attained the breakthrough which could mean the adsorption column could have turned to the reactor. The rate-controlling mechanism was found to be the reaction between silver and iodine. XRD analysis supports the loading by a chemical mechanism. I_2 has been detected at the exit of the column in which sodium mordenite was loaded as an adsorbent.

5.2 Future work

In research to effective capture of the iodine species, there are still several parameters that need to be investigated. More economic and stable adsorbents should be used in the capture of iodine species. Silver mordenite is found as an effective adsorbent. This research helps to prove this point as well. The future work includes more parametric studies on adsorbent such as the effect of moisture on the adsorbent, effect of contaminants such as NO_X, the material of construction, the effect of different temperatures, desorption cycles, sorbent regeneration cycles which can give information about the efficacy of the adsorbent and adsorbent aging.

References

[1]World Nuclear Association, "World Nuclear Performance Report", report number 2020/008, August 2020.

[2]U.S. Department of Energy, "The Ultimate Fast Facts Guide to Nuclear Energy", 2020, https://www.energy.gov/ne/office-nuclear-energy.

[3]Baron J. et al, "Public Opinion on Nuclear Energy and Nuclear Weapons: The Attitudinal nexus in the United States", *Energy Research and Social Science*, vol. **68**, October 2020, https://doi.org/10.1016/j.erss.2020.101567.

[4]Nuclear Energy Institute, "Nuclear by the numbers", August 2020, https://www.nei.org//resources/fact-sheets/nuclear-by-the-numbers accessed December 2020.

[5]U.S.NRC, "Power Reactors", https://www.nrc.gov./reactors/power.html accessed December 2020.

[6]Lau L. et al, "Is nuclear energy clean? Revisit of Environmental Kuznets Curve hypothesis in OECD countries", *Economic Modelling*, vol. **77**, pp. 12–20, Mar. 2019, doi: 10.1016/j.econmod.2018.09.015.

[7]Boccard N., "Capacity Factor of Wind Power: Realized Values vs. Estimates", *Energy Policy*, vol. **37**, Issue no. 7, pp. 2679-2688, July 2009, doi: 10.1016/j.enpol.2009.02.046.

[8]Marques J. et al, "Evolution of Nuclear Fission Reactors: Third Generation and Beyond", *Energy Conversion and Management*, vol. **51**, no. 9, pp. 1774–1780, Sep. 2010, doi: 10.1016/j.enconman.2009.12.043.

[9]Lamarsh J. et al, *Introduction to nuclear engineering*, 3rd ed. Upper Saddle River, N.J: Prentice Hall, 2001.

[10]Openstax, "University Physics III - Optics and Modern Physics", https://phys.libretexts.org/Bookshelves/University_Physics/Book%3A_University_Physics_(OpenStax)/Map%3A_University_Physics_III_-_Optics_and_Modern_Physics_(OpenStax), accessed December 2020.

[11]Olvera-Guerrero O. et al, "Non-Linear Stability Analysis of Real Signals from Nuclear Power Plants (Boiling Water Reactors) Based on Noise Assisted Empirical Mode Decomposition Variants and the Shannon Entropy", *Entropy*, vol. **19**, no. 7, pp. 359-391, Jul. 2017, doi: 10.3390/e19070359.

[12]Zohuri B. et al, "Nuclear Fuel Cycle and Decommissioning", Nuclear Reactor Technology Development and Utilization, *Woodhead Publishing Series in Energy*, pp. 61–120, 2020. https://doi.org/10.1016/B978-0-12-818483-7.00002-0.

[13]Schneider E. et al, "Measures Of The Environmental Footprint Of The Front End Of The Nuclear Fuel Cycle", *Energy Economics*, vol. **40**, pp. 898–910, Nov. 2013, doi: 10.1016/j.eneco.2013.01.002.

[14]The U.S.NRC, "Spent Fuel Storage - Spent Fuel Pools", https://www.nrc.gov/waste/spent-fuel-storage/pools.html, accessed December 2020.

[15]U.S.NRC, "Spent Fuel Storage - Dry Cask Storage", https://www.nrc.gov/waste/spent-fuel-storage/dry-cask-storage.html, accessed December 2020.

[16]Jubin R., "Spent Fuel Reprocessing", *Vanderbilt University CRESP III*, pp. 127-148, April 2009.

[17]Castano C., "Nuclear Fuel Reprocessing", *Nuclear Energy Encyclopedia: Science, Technology and Applications*", pp. 121-126, June 2011, doi: 10.1002/9781118043493.ch14.

[18]Simpson M., "Nuclear Fuel Reprocessing Technologies and Commercialization", *Science and Technology of Nuclear Installations*, vol. **2013**, Article ID 815693, 2 pages, August 2013. https://doi.org/10.1155/2013/815693.

[19]Pandey N. et al, "PUREX and THOREX Processes (Aqueous Reprocessing)", *Reference Module in Materials Science and Materials Engineering*, 2016, https://doi.org/10.1016/B978-0-12-803581-8.02094-4.

[20]Laidler J. et al, "Development of Pyroprocessing Technology", *Progress in Nuclear Energy*, vol. **31**, issues 1-2, pp. 131-140, 1997, https://doi.org/10.1016/0149-1970(96)00007-8.

[21]Lee H. *et al.*, "Pyroprocessing Technology Development at KAERI", *Nuclear Engineering and Technology*, vol. **43**, pp. 317-328, August 2011, doi: 10.5516/NET.2011.43.4.317.

[22]Ewing R. et al, "Nuclear Waste Management in the United States-Starting Over", *Science*, vol. **325**, issue no. 5937, pp. 151–152, Jul. 2009, doi: 10.1126/science.1174594.

[23]Haefner D., "Methods of Gas-Phase Capture of Iodine from Fuel Reprocessing Off-Gas: A Literature Survey," INL/EXT-07-12299, 911962, Feb. 2007. doi: 10.2172/911962.

[24]"A reflux method pictures", https://goldbamboo.com, accessed December 2020.

[25]Lin M., "Studies of the Effects of Electrolyte Additives on the Reactivity Between Charged Electrodes and Electrolytes in Li-Ion Batteries Using Accelerating Rate Calorimetry", *A thesis for master of science*, Dalhousie University, July 2014,

[26]U.S. EPA. 1996. "Method 3050B: Acid Digestion of Sediments, Sludges, and Soils," Revision 2. Washington, DC.

[27]Valco Instruments Co. Inc, "An Instruction Manual of Dynacalibrator Model 230", https:// www.vici.com/support/manuals/dyna230.pdf accessed December 2020.

[28]KIN-TEK Analytical, Inc, "How Permeation Tubes Work", https://kin-tek.com, accessed December 2020.

[29]Valco Instruments Co. Inc, "Backflush of Precolumn to Vent with a Valco 6 port valve", https://www.vici.com, accessed December 2020.

[30]Bruffey et al, "Capture of Elemental and Organic Iodine from Dilute Gas Streams by Silver-exchanged Mordenite," *Procedia Chemistry*, vol. **21**, pp. 293–299, January 2016, doi: 10.1016/j.proche.2016.10.041.

[31]Scheele R. et al, "Methyl Iodide Sorption By Reduced Silver Mordenite", *A technical report prepared for DOE*, report no PNL-4489,1983, doi: 10.2172/6017408.

[32]Nenoff T. et al, "Silver-Mordenite For Radiologic Gas Capture From Complex Streams: Dual Catalytic CH_3I Decomposition and I Confinement", *Microporous and Mesoporous Materials*, vol. **200**, pp. 297–303, Dec. 2014, doi: 10.1016/j.micromeso.2014.04.041.

[33]Joffrey H. et al, "Porous Sorbents for the Capture of Radioactive Iodine Compounds: A Review", *RSC Advances*, vol. **8**, issue no 51, pp. 29248-29273, 2018, doi: 10.1039/C8RA04775H.

[34]Soelberg N. et al, "Radioactive Iodine and Krypton Control For Nuclear Fuel Reprocessing Facilities", *Science and Technology of Nuclear Installations*, vol. **2013**, Article ID 702496, 12 pages, July 2013, https://doi.org/10.1155/2013/702496.

[35]Juhola A., "Iodine Adsorption and Structure of Activated Carbons," *Carbon*, vol. **13**, issue no. 5, pp. 437–442, 1975, doi: 10.1016/0008-6223(75)90016-0.

[36]Nan Y. et al, "Adsorption of Iodine on Hydrogen-Reduced Silver-Exchanged Mordenite: Experiments and Modeling," *AIChE J.*, vol. **63**, issue no. 3, pp. 1024–1035, Mar. 2017, doi: 10.1002/aic.15432.

[37]Jubin R., "The Mass Transfer Dynamics of Gaseous Methyl Iodide Adsorption by Silver-Exchanged Sodium Mordenite," ORNL--6853, 161458, Dec. 1994. doi: 10.2172/161458.

[38]Chebbi M. et al, "A Combined DRIFTS and DR-UV–Vis Spectroscopic In Situ Study on the Trapping of CH_3I by Silver-Exchanged Faujasite Zeolite", *The Journal of Physical Chemistry*, vol. **120**, issue no. 33, pp. 18694–18706, Aug. 2016, doi: 10.1021/acs.jpcc.6b07112.

[39]Park S. et al, "Adsorption Behavior of Methyl Iodide on a Silver Ion-Exchanged ZSM-5", *Microporous and Mesoporous Materials*, vol. **294**, p. 109842, 2019, doi: 10.1016/j.micromeso.2019.109842.

[40]Riley B. et al, "Materials and Processes For the Effective Capture and Immobilization of Radioiodine: A review", *Journal of Nuclear Materials*, vol. **470**, pp. 307–326, Mar. 2016, doi: 10.1016/j.jnucmat.2015.11.038.

[41]Choi B. et al, "Adsorption Equilibrium and Dynamics of Methyl Iodide in a Silver Ion-Exchanged Zeolite Column at High Temperatures", *Adsorption*, vol. **7**, pp. 91-103, 2001.

[42]Asmussen R. et al, "Silver-Functionalized Silica Aerogels and Their Application in the Removal of Iodine from Aqueous Environments", *Journal of Hazardous Materials*, vol. **379**, January 2018, https://doi.org/10.1016/j.jhazmat.2018.04.081.

[43]Subrahmanyam K. et al, "Chalcogenide Aerogels as Sorbents for Radioactive Iodine", *Chemistry of Materials*, vol. **27**, issue no 7, pp. 2619-2626, April 2015. doi: 10.1021/acs.chemmater.5b00413.

[44]Valizadeh B. et al, "Porous Metal-Organic Framework@Polymer Beads for Iodine Capture and Recovery Using a Gas-Sparged Column", *Advanced Functional Materials*, vol. **28**, p. 1801596, issue no 30, July 2018, https://doi.org/10.1002/adfm.201801596.